CZECH UNIVERSITY OF LIFE SCIENCES PRAGUE
FACULTY OF ENVIRONMENTAL SCIENCES

DEPARTMENT OF WATER RESOURCES
AND ENVIRONMENTAL MODELING

THE EFFECT OF THE NEWLY ESTABLISHED SILVO-ARABLE AGROFORESTRY SYSTEM ON THE SOIL MOISTURE AND TEMPERATURE REGIME OF THE AMÁLIE LOCATION

BACHELOR THESIS

Supervisor: Ing. Lukáš Jačka, Ph.D.
Student: Helena Chalupecká

2024

CZECH UNIVERSITY OF LIFE SCIENCES PRAGUE

Faculty of Environmental Sciences

BACHELOR THESIS ASSIGNMENT

Helena Chalupecká

Water Management

Thesis title

The effect of the newly established silvo-arable agroforestry system on the soil moisture and temperature regime of the Amálie location

---

Objectives of thesis

The main aim is to evaluate the effects of the silvo-arable agroforestry system at the Amálie site on the soil moisture and temperature regime during the first year after establishment. A sub-aim is to establish continuous monitoring using the autonomous microclimatic TMS Tomst stations.

Methodology

To prepare a detailed literature review focusing on various agroforestry systems' hydrological and microclimatic functions, emphasizing the silvo-arable systems. As part of the literature review, describe the soil's elementary hydro-physical properties (especially soil moisture, bulk density, and texture) and how they are determined.

In the practical part, participate in establishing the continuous monitoring of soil moisture and temperature in an agroforestry system and a nearby control soil using the TMS Tomst microclimatic stations. Also, collect undisturbed soil samples for reference determination of soil moisture and bulk density and disturbed samples for particle size distribution analysis. Furthermore, evaluate the soil moisture and temperature data for the entire monitoring period and compare the forested strips in the agroforestry system with the unaffected control soil.

The proposed extent of the thesis

35 pages

Keywords

silvoarable alley cropping system, integration of trees, arable land, modification of microclimate, soil-water status

---

Recommended information sources

Jacobs, S.R., Webber, H., Niether, W., Grahmann, K., Lüttschwager, D., Schwartz, C., Breuer, L., Bellingrath-Kimura, S.D., 2022. Modification of the microclimate and water balance through the integration of trees into temperate cropping systems. Agric. For. Meteorol. 323, 109065.

Rolo, V., Rivest, D., Maillard, É., & Moreno, G., 2023. Agroforestry potential for adaptation to climate change: A soil-based perspective. Soil Use and Management 39, 1006–1032.

Šinko, J., Weger, J., 2023. Monitoring mikroklimatických podmínek a hydrického režimu silvoorebného agrolesnického systému – první výsledky. In: Hnilicová, S., Tesař, M. (Eds.), Hydrologie malého povodí 2023. Ústav pro hydrodynamiku AV ČR, v. v. i., s. 131-140, Praha, ISBN 978-80-87117-22-4.

Expected date of thesis defence

2023/24 SS – FES

The Bachelor Thesis Supervisor

Ing. Lukáš Jačka, Ph.D.

Supervising department

Department of Water Resources and Environmental Modeling

Advisor of thesis

Ing. Martin Kovář

Electronic approval: 22. 2. 2024

prof. Ing. Martin Hanel, Ph.D.

Head of department

Electronic approval: 23. 2. 2024

prof. RNDr. Michael Komárek, Ph.D.

Dean

Prague on 07. 03. 2024

I hereby declare that I have independently elaborated the bachelor/final thesis with the topic of: The effect of the newly established silvo-arable agroforestry system on the soil moisture and temperature regime of the Amálie location, and that I have cited all of the information sources that I used in the thesis as listed at the end of the thesis in the list of used information sources.

I am aware that my bachelor/final thesis is subject to Act No. 121/2000 Coll., on copyright, on rights related to copyright and on amendments of certain acts, as amended by later regulations, particularly the provisions of Section 35(3) of the act on the use of the thesis.

I am aware that by submitting the bachelor/final thesis I agree with its publication under Act No. 111/1998 Coll., on universities and on the change and amendments of certain acts, as amended, regardless of the result of its defence.

With my own signature, I also declare that the electronic version is identical to the printed version and the data stated in the thesis has been processed in relation to the GDPR.

In Prague on .....

Helena Chalupecká

ACKNOWLEDGEMENTS

I would like to express my gratitude to my thesis supervisor, Ing Lukáš Jačka, Ph.D., whose guidance, academic encouragement, and insightful discussions have been invaluable throughout the course of my thesis.

I would also like to extend my sincere thanks to the hydropedology team, particularly my advisor, Ing. Martin Kovář, Jakub Machuta, and Ing. Marta Kuželková. Their collaborative efforts and support in installation of the TOMST monitors, as well as their invaluable assistance with both field and laboratory measurements, have been a cornerstone of my research.

Finally, I would like to thank Prof. Ing. Bohdan Lojka, Ph.D. and Ing. Daniel Preininger for their support of agroforestry monitoring project in Amálie.

ABSTRACT

Coupled with the increasing convergence of dry spells and high temperatures, agricultural intensification has made cropping systems more vulnerable to environmental changes. Agroforestry, a sustainable land use system that combines tree cultivation and agricultural production on the same plot, emerges as a solution to these challenges, offering benefits such as improved soil quality and fertility, erosion prevention, enhanced water management, biodiversity conservation, microclimate regulation, and climate change mitigation through carbon sequestration.

This study used a total of 36 microclimatic stations to monitor and assess the influence of a newly implemented agroforestry system in the Amálie location on the soil temperature and moisture regime at, above, and below the soil surface. The resulting data exhibited lower temperature amplitudes in forested alleys, with the most significant differences seen in peak temperatures, particularly during the heatwaves in August. On average, temperatures at and beneath the surface were 3ºC and 4ºC cooler in the forested alleys compared to the crop fields. The study also found that forested alleys reacted more swiftly and significantly to precipitation events, with the volumetric soil moisture content at 8 cm below ground being 7% higher in tree rows than in crop fields. However, due to the rapid water uptake by trees, the moisture content beneath them quickly plummeted, resulting in consistently lower soil moisture in forested alleys compared to crop fields. This trend persisted even at a depth of 25 cm, where the soil moisture content remained consistently lower even after rainfall events.

Although the silvoarable agroforestry system implemented in Amálie may initially exert a negative impact on the soil moisture regime, its microclimatic advantages and capacity to improve water management through the alteration of soil properties, reduction of runoff, and enhanced preferential flow, are substantial. As the trees mature, they hold the potential to enhance the resilience of the studied agroforestry system, making it less susceptible to weather extremes brought on by climate change.

KEYWORDS: silvoarable alley cropping system, integration of trees, arable land, modification of microclimate, soil-water status

TABLE OF CONTENTS

1. INTRODUCTION

In response to the rapid population growth during the latter half of the twentieth century, the necessity for greater agricultural yield led to the utilization of fertilizers, pesticides, and genetically modified crops in monocultural crop systems, fostering a product-driven approach to agroecosystems. Albeit successful in catering to the growing demand, the process of agricultural intensification led to the development of unsustainable agricultural practices that detrimentally impacted soil health and productivity by exacerbating issues such as erosion, compaction, contamination, and organic matter deficits (Horrigan et al., 2002; Mbow et al., 2014; Rolo et al., 2023). Combined with the increasing frequency of compound events, characterized by the convergence of prolonged droughts and high temperatures, the effects of agricultural intensification could pose a significant threat to cropping systems, making them more susceptible to environmental and climatic changes (Barrios et al., 2015; Sedlmeier et al., 2018; Jacobs et al., 2022).

Given the continuous evolution of social, institutional, and environmental pressures, it is necessary to implement more resilient and diversified cropping systems with a greater self-regulatory capacity (Beillouin et al., 2020; Sedlmeier et al., 2018; Lüttger and Feike, 2018; Webber et al., 2020; Paul et al., 2017). In this context, agroforestry, a land use system that combines tree cultivation and agricultural production on the same plot of land, emerges as a promising strategy. It not only holds the potential to enhance yield stability but also offers a multitude of benefits such as the enhancement of soil quality and fertility, prevention of erosion, improved water management, conservation of biodiversity, regulation of microclimate, and mitigation of climate change through carbon sequestration (Young, 1997; Jose, 2009; Nuberg et al., 2009; Powlson et al., 2011; Nair and Garrity, 2012).

Although agroforestry has garnered global attention as a sustainable alternative to conventional agricultural systems amidst climate change (Nair, 2007), its impact on the moisture and temperature regimes of specific soil types remains insufficiently studied. This thesis aims to bridge this knowledge gap by helping answer the question of whether forested alleys within agroforestry systems can effectively manage water resources and moderate temperature extremes in silt loam soils.

2. AIMS OF THESIS

The primary objective of this thesis is to assess the impact of the silvo-arable agroforestry system on the soil moisture and temperature regime in the Amálie location during the inaugural year following its establishment. Additionally, this thesis aims to implement continuous monitoring through the installation of the TMS Tomst, an autonomous microclimatic station.

3. LITERARY REVIEW

3.1. Defining soil and its significance

Soil is integral to life on Earth, defining the nature of plant ecosystems and the ability of land to support animal life and society. Its significance, however, goes beyond the historically prevalent understanding of soil as a plant-growth medium with a purely productive capacity. Soil plays an important role in the ecosystem, regulating many biotic processes, cycles, and the transportation and flow of substances in nature (Tomášek, 2007). It provides physical support for plant root systems and governs biogeochemical processes essential for nutrient cycling. It regulates and retains water supplies within its pores, impacting the quality and quantity of water that is infiltrated into and transported by soil. Moreover, soil stores and transforms organic matter, contributing to biogeochemical cycles and influencing climatic phenomena such as the greenhouse effect (Weil and Brady, 2016).

Soil is formed through the process of weathering on the upper layer of Earth's solid surface. Given time and the effects of the atmosphere, hydrosphere, and relief (elevation, slope of terrain, orientation), the soil's parent materials (original minerals forming the Earth's solid surface) yield weathered materials. Although weathered material does not inherently qualify as soil, it is a prerequisite for its formation. The process of soil formation begins when the activity of organisms, namely microorganisms, vegetation and edaphon, is added to the erosive forces. Altogether, these pedogenetic factors and processes create soil, a dynamic ecosystem that forms, evolves, and is maintained under the influence of the surrounding environment. As defined by V.V. Dokuchaev, soil is an "independent natural and historical formation that arises from and develops through a lawful process, defined by a combination of several soil-forming factors" (Tomášek, 2007). A similar definition was drawn up by Kutílek (1978), who defined soil as a "natural formation created at the interface of the lithosphere with the atmosphere or hydrosphere through the combination of pedogenetic factors in the pedogenetic process. Soil is biologically active and differentiated into horizons."

3.1.1. Soil as a three-phase system

Soil can be viewed as an open biogeochemical system made up of three states of matter that are in constant interaction with one another. The solid phase, also known as the soil matrix, is comprised of minerals and organic matter. The pores within the soil matrix hold the final two phases: the gaseous phase (soil atmosphere), and the liquid phase (soil solution) (Šimek, 2003).

Solid phase

The solid phase of the soil is primarily made up of discrete particles formed through the weathering of parent minerals and soil-forming substrates, constituting a mixture of rock fragments and minerals. These particles, ranging in size from larger stones to sand, silt, and clay particles, also have varying mineral compositions and play a crucial role in the chemical and physical characteristics of soil. The minerals most abundantly represented in soil are silicates, oxides, hydroxides, carbonates, phosphates, chlorides, sulfides, and sulfates (Weil and Brady, 2016; Šimek, 2003). The second component of the soil matrix is the organic matter. Organic matter contains various carbonaceous substances, including living organisms (soil biomass), the remains of microorganisms, plants, and animals, as well as organic compounds produced by current and past metabolism in the soil (humus). Although organic matter constitutes a small (1-6%) fraction of soil make-up, it plays a crucial role in its physical and chemical properties by impacting granular structure, water retention, nutrient availability, and biochemical activity (Hillel, 2004; Weil and Brady, 2016).

Soil solution

Soil water can be defined as an aqueous solution with a variable chemical composition determined by the exchanges of matter and energy between the soil atmosphere, minerals, and biota. It not only stands as a vital source of nutrients for plants, deriving its nutrient elements from fine organic and inorganic colloidal particles, such as clay and humus, from the soil matrix, but also serves as a chemical buffer. The protonation of minerals and organic material in soil water enhances the soil's resilience to pH fluctuations even in the presence of acidifying or alkalizing factors. Beyond its pH, soil water can also be characterized by its chemical composition; the main inorganic components among cations include calcium,

magnesium, potassium, and sodium ions, while the predominant anions include sulfate, nitrate, bicarbonate, and chloride ions. Major organic components consist of carboxylic acids, amino acids, and simple sugars. Overall, one of the principal characteristics of soil is its water content (Weil and Brady, 2016; Sposito, 2016; Šimek, 2003).

Soil atmosphere

The soil atmosphere is defined as the gases occupying pores that are not entirely or are only partially filled with soil water. Soil pores are filled with air due to drainage or when water is extracted through evaporation or root absorption. The composition of the soil atmosphere varies temporally and spatially and differs significantly from the atmosphere above ground. This disparity is most notably due to the elevated levels of carbon dioxide, which can be 10-100% higher than the concentration of carbon dioxide in the atmosphere (0.15-10% of the soil volume) depending on the connectivity of pores with the atmosphere above ground. Elevated concentrations of CO2 occur especially in areas with increased microbial activity and near plant roots. Another major difference between the soil atmosphere and the atmosphere above ground is the low oxygen content, ranging from trace amounts, to 20% of the soil volume. Moreover, the water vapor content of soil air is consistently high, often exhibiting a relative humidity over 98% (Weil and Brady, 2016; Hillel, 2004; Šimek, 2003).

3.1.2. Soil morphology and taxonomy

The formation of soil is impacted by a series of factors and conditions; factors have a direct effect on the soil-formation process and include the parent material, climate, biota, groundwater, and human influence. Conditions, on the other hand, affect the soil-formation process by influencing the factors. They include the relief (slope, orientation, elevation), and time (Tomášek, 2007).

The basis of the soil formation process is the parent material, otherwise known as the soil-forming substrate. It can be defined as the unconsolidated and chemically weathered mineral from which a soil is developed through pedogenic processes. The petrological composition of the parent material impacts the time required for soil formation, the associated soil depth, and the granulometric composition, which

projects itself into many other physical, physiochemical, and biological properties of the resulting soil (Weil and Brady, 2016; Tomášek 2007).

The aforementioned factors and conditions give way to the soil forming processes during which the originally inert parent mineral transforms into soil. We distinguish the following rudimentary soil-forming processes: weathering, humification, eluviation and illuviation, gleization and salinization. Soils that undergo the same soil-forming processes and are developed under a specific set of factors and conditions can be defined and grouped by similar morphological and analytical features into soil types. The most common soil types found in the Czech Republic include: chernozems, phaeozems, vertisols, greyic phaeozems, haplic luvisols, albeluvisols, stagnosols, lithic leptosols, rendzic leptosols, terra fusca, leptosols, arenosols, pelosols, cambisols, entic podzols, haplic podzols, fluvisols, gleysols, histosols, and saline soils (Tomásek, 2007; Němeček, 2002). Due to the scope of this thesis, this chapter will only touch on the two soil types that are found in the studied area of Amálie: cambisols and albeluvisols.

Cambisols

Cambisols are the most widespread soil type in the Czech Republic, covering almost 50% of the nation's land. This soil type developed under original deciduous and mixed forests from a wide range of parent substrates, including granite, gneiss, schist, phyllite, basalt, sandstone, and shale (Němeček, 1990). They can be found in predominantly humid, mildly warm areas with annual precipitation ranging between 500-900 mm and an average temperature of 4-9ºC. The relief that they occur in can be characterized as the slopes, peaks, and ridges of hilly areas, highlands, and even mountains, with elevations in the range of 450-800 meters above sea level (Vopravil, 2010).

The primary soil-forming process of this soil type is intrasoil weathering, which is made evident through the browning of the B horizon – a characteristic trait of cambisols, caused by the release of iron and aluminum from the crystalline lattice of minerals in a process called brownification (Němeček, 1990; Vopravil, 2010). As portrayed by Fig. 1, beneath the humic horizon lies the brown to rust brown Bv horizon, which is where the intense intrasoil weathering take place. The cambic horizon then transitions into a lighter and less weathered soil-forming substrate in the

C horizon with a pronounced gradation. This transitional horizon between Bv and C is labeled as B/C (Tomášek, 2007; Vopravil, 2010; Pavlů, 2018).

The prevalent subtypes of cambisols in the Czech Republic are haplic, luvic, stagnic, hyperdystric, arenic, and pelic cambisols, differing in their parent substrate, which heavily impacts the soil's chemical and physical characteristics. Haplic cambisols, found in the studied area of Amálie, develop from parent substrates within the heavy to light medium soil texture class. More specifically, the haplic cambisol soil found in the studied area is of the eubasic variety, signifying that the saturation of the sorption complex in its Bv horizon is greater than 50% (Němeček et al., 2002; Vopravil, 2010).

Albeluvisols

Albeluvisols developed predominantly under acidic oak and beech forests. The parent substrates are most commonly loess soils, moderately heavy glacial sediments, stratified slope deposits, sometimes even clayey terrace sediments (Vopravil, 2010; Tomásek, 2007). Albeluvisols can be found in humid areas with annual precipitation ranging between 600-900 mm and an average temperature of 6-8ºC. The relief that they occur in can be characterized as the valleys of gently undulating, or distinctly rolling hills and highlands, with elevations in the range of 300-600 meters above sea level (Tomášek, 2007; Kutílek, 1978).

The main soil-forming process is illimerization, making albeluvisols a variation of illimerized soils. As evident in Fig. 2, illimerization leads to the formation of a bleached eluvial horizon (E) with a platy to blocky structure. The eluvial zone is developed through eluviation, a process caused by the transport of the soil's highly dispersive clay fraction, as well as the coating of non-silicate iron and aluminum that are found in the upper layer of the soil. Due to the downward percolation of water across the soil horizons, the transported material, or the iluvial deposit, is then accumulated in the lower layers of the soil. The resulting enriched iluvial deposit is rust-brown in color and has a prismatic structure (Vopravil, 2010; Tomášek, 2007; Pidwirny, 2008).

A common occurrence in albeluvisols is the formation of a gley horizon in the lower layers of the soil profile above the parent material in a process called gleization. It is a process wherein the clay-enriched illuvial horizon creates a waterlogged

environment due to its impermeability to water, causing retention atop the layer surface. The poor drainage conditions and a lack of oxygen lead to the concentration of hydrated iron and manganese oxides into small, dark, rust-colored concretions, or nodules, which are abundant in the bleached eluvial horizon (Bockheim, 2017; Vopravil, 2010).

The prevalent subtypes of albeluvisols in the Czech Republic are haplic, stagnic, dystric, and arenic albeluvisols. Haplic albeluvisols, found in the studied area of Amálie, are developed from moderately heavy parent substrates (Vopravil, 2010).

Fig. 1: Cambisol soil profile (modified from Tomášek, 2007)

Fig. 2: Albeluvisol soil profile (modified from Tomášek, 2007)

3.2. Physical characteristics of soil

3.2.1. Particle density

Particle density (ρ_M) represents the mass of a unit volume of the solid matter in a sample of soil. Its resulting value is therefore determined by the mineral composition and content of organic material. To measure particle density, a disturbed soil sample is extracted and then dried to remove any water. Once dry, the sample is

inserted into a pycnometer, where the volume of the solid matter is determined through the application of Archimedes' principle. After acquiring the volume of the solid matter, the following equation is used to calculate the particle density (ρ_M) of the soil sample:

$$\rho_M = \frac{m_M}{V_M} = \frac{m_M}{m_{pw}+m_M+m_{ps}} \quad (1)$$

Where m_M and V_M are the mass [g] and volume [cm^3] of the dry solid phase respectively, m_{pw} is the mass of the pycnometer filled with water [g], and m_{ps} is the mass of the pycnometer containing the suspension [g] (Pavlásek and Jačka, 2014; Semnani, 2016).

Particle density is a soil characteristic that remains practically constant in a specific location over time. In mineral soils, the average value of particle density is within the range of 2.6-2.7 g·cm^{-3}. In practice, most inorganic mineral soils have an estimated particle density of 2.65 g·cm^{-3} due to the high concentration of quartz in most soils. Soils containing more dense minerals, such as hematite and limonite, can have a particle density of over 2.7 g·cm^{-3}. On the other hand, less dense minerals, such as montmorillonite or kaolin, can decrease the particle density of soils to 2.5 g·cm^{-3}. Particle density can reach the value of 1.0 g·cm^{-3} in the organogenic horizon of forest soil, especially in the leaf litter horizon of deciduous trees (Pavlásek and Jačka, 2014; Rejšek and Vácha, 2018).

3.2.2. Soil bulk density

Soil bulk density (ρ_s) represents the weight of soil in a given volume, which is dependent on the percentual make-up and density of the soil matrix (solid phase), and the volume of soil pores. Soil bulk density (ρ_s) is expressed by the equation:

$$\rho_s = \frac{m_M}{V_s} \quad (2)$$

Where m_M represents the mass of the solid phase of the soil [g] and V_s is the volume of the soil sample [cm^3]. Soil bulk density is determined based on the weight of a dried, undisturbed soil sample of known volume, where the weight, excluding that of the gaseous phase, equals the mass of the soil phase of the soil (Pavlásek and Jačka, 2014).

Bulk density is always lower than particle density and is influenced by granulometric composition, particularly the skeletal grain fraction and the size of its particles, as well as the structure and porosity of the soil (Rejšek, Vácha, 2018). To elaborate, the relationship between soil bulk density and porosity is inversely proportional. As such, soils that lack structure, namely single-grained and massive soil (sandy and sandy loam soil), typically exhibit a bulk density ranging from 1.6-1.7 $g \cdot cm^{-3}$. As the structure of the soil develops, soil aggregates form, creating pores known as interped spaces. Interped spaces lead to increased porosity, thereby lowering the bulk density. A value of 1.450 $g \cdot cm^{-3}$ is considered typical for loam surface soils with a granular structure. With the increase of organic matter in soil, the porosity rapidly increases; bulk density values in organogenic soils with minimal mineral content such as peat can reach as low as 0.2 $g \cdot cm^{-3}$. The relationship between the granulometric composition of soil and soil bulk density can be seen in Table 1 (Rejšek and Vácha, 2018; Foth, 1990; Pavlásek and Jačka, 2014).

Table 1: Critical bulk densities (modified from Lhotský, 2000)

Textural soil classification	**% of particles below 0,01 mm**	**Soil bulk density [$g\ cm^{-3}$]**
Clay	>75	>1.35
Clay loam	75-46	>1.4
Loam	45-39	>1.45
Sandy loam	30-21	>1.55
Loamy sand	20-11	>1.6
Sand	>10	>1.7

Soil bulk density is not constant, it is therefore essential to assess it for each measurement of hydrophysical properties, especially for different soil conditions, seasons, and stages of vegetation development. Its value changes depending on the depth of soil horizons, soil biota activity, moisture, and temperature fluctuations. Human activity, especially agricultural practices (plowing, field cultivation, and use of heavy machinery) also greatly impact bulk density (Pavlásek and Jačka, 2014).

3.2.3. Porosity

Soil porosity (P) describes the soil pore system in terms of its volume relative to the total volume of soil. It is a dimensionless characteristic, which can be determined using the formula:

$$P = \frac{V_p}{V_s} = \frac{V_A + V_W}{V_A + V_W + V_M} \quad (3)$$

Where V_p represents the nonsolid volume [m^3], V_s is the total volume of the soil [m^3], V_A is the volume of the soil atmosphere [m^3], V_w is the volume of the soil solution [m^3], and V_M is the volume of solid phase of the soil [m^3] (Pavlásek and Jačka, 2014; Kutílek and Nielsen, 1994).

Porosity is often determined based on previously measured particle and soil bulk density:

$$P = \frac{\rho_M - \rho_S}{\rho_M} = 1 - \frac{\rho_S}{\rho_M} \quad (4)$$

Where ρ_M represents particle density [$kg \cdot m^{-3}$] and ρ_S represents soil bulk density [$kg \cdot m^{-3}$] (Pavlásek and Jačka, 2014).

The porosity of soils is highly variable and is dependent on particle arrangement, soil texture (Table 2) and structure, organic matter content, and genetic horizon. It is also dependent on anthropogenic factors and seasonal variations, such as the activity of organisms, plant growth intensity, and temperature fluctuations (Pavlásek and Jačka, 2014; Kutílek and Nielsen, 1994; Foth, 1990).

Table 2: Porosity values for mineral soils (modified from Schatschabel et al., 1984)

Textural soil classification	Porosity [%]
Sandy soil	56 - 36
Silty soil	56 - 39
Loamy soil	55 - 30
Clayey soil	70 - 35

The soil pore system is often analyzed using models of soil moisture retention curves, where the actual pore radius is substituted by an equivalent pore radius. Based on the equivalent radius, and the principles of hydrostatics and hydrodynamic, pores can then be classified as micropores with an equivalent radius below 1μm, capillary

pores with an equivalent radius ranging from 1μm to 1mm, and macropores with an equivalent radius greater than 1mm. The size of the pores in the soil has a substantial impact on water retention capacity. For example, sandy soils, despite having a lower porosity than clayey soils, allow for faster percolation of water due to their difference in pore sizes. Sands primarily consist of macropores, which are often referred to as aeration pores due to their inability to retain water against gravity. Conversely, fine-textured clayey soils, rich in micropores, have a large water retention capacity, but lack the ability to drain water due to meniscus forces (Kutílek and Nielsen, 1994; Gerrard, 2000; Foth, 1990).

The nature of a soil pore system and its interconnectivity influences several physical characteristics of the soil. As illustrated by equation 4, porosity and soil bulk density have an inverse relationship. Porosity is also linked to soil permeability and various processes within the soil, such as gas diffusion, and substance transport, making it an integral characteristic in agronomy (Pavlásek and Jačka, 2014; Kutílek and Nielsen, 1994; Prasad and Pietrzykowski, 2020).

3.2.4. Soil structure

Soil structure can be characterized through the size, shape, and spatial arrangement of soil particles, soil aggregates, and interped spaces (Gerrard, 2000).

Soil aggregates, or peds, form through the grouping of elementary soil particles of various sizes. One of their fundamental characteristics is their water retention capacity, setting them apart from pseudo-aggregates, or clods, which are a result of compaction by heavy agricultural machinery and long-term tillage. Soil aggregates are distinguished by size; microaggregates are smaller than 250μm, while macroaggregates constitute the remaining peds that are larger than 250μm in diameter (Šarapatka, 2014; Kutílek, 1978; Ciric et al., 2012).

Soil microaggregates form primarily through the clustering of soil particles of various particle size fractions due to the coagulation of soil colloids. In addition to the coagulation, sesquioxide gels, such as Fe_2O_3 and Al_2O_3, amorphous coatings on the surface of mineral particles, humic acids, and other organic substances, also contribute to the formation of microaggregates (Kutílek, 1978).

On the other hand, macroaggregates are dependent on the process of micro-aggregation, forming through the enlargement and clustering of microaggregates. The formation of macroaggregates is also heavily influenced by processes taking place within the soil, including changes in soil temperature and volume, soil tillage, and the mechanical and biological activity of soil biota (namely edaphones) and plant root systems (Kutílek 1978; Pavlásek and Jačka, 2014).

Soil structure can be classified based on its developmental stage and shape of soil aggregates. In terms of development, the first category of soils are non-structured soils with no discernable signs of particle aggregation, or with the presence of pseudo-aggregates. The second category constitutes soils with a weakly developed structure in which signs of particle aggregation can be observed, but non-structured material still predominates. Lastly, the third category represents soils with a pronounced structure, characterized by a significant presence of soil macroaggregates (Kutílek, 1978).

Soils can be classified into four primary morphological classes based on the shape of their macroaggregates:

Class I. aggregates are rounded, with all three axes of equal length. The following types of class I structures are distinguished: granular (Fig. 3a), crumb (Fig. 3b), single grain (Fig. 3c), and structureless (Fig. 3d). Granular structure aggregates, unlike crumb aggregates, are slightly larger in size. Structureless and single grain aggregates belong to the first and second developmental category; single grain soils show no aggregation of coarse particles when dry, while structureless soils show no aggregation of fine particles when dry. Such soils are highly permeable and are commonly found in the A horizon due to the activity of zooedaphones.

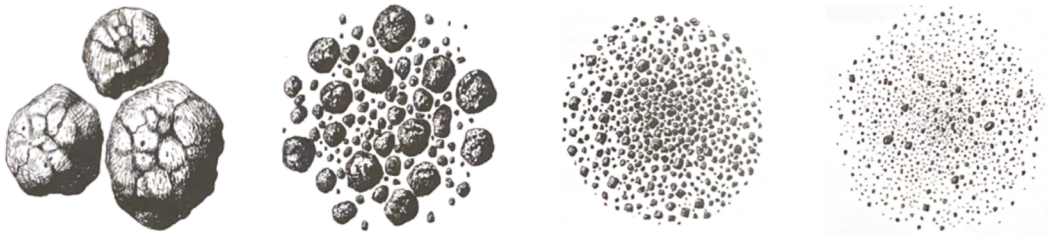

A) Granular B) Crumb C) Single grain D) Structureless

Fig. 3: Types of soil structures within class I (Tomášek, 2007)

Class II. aggregates exhibit distinct surfaces and edges, with all three axes of equal length. The following types of structures within this class differ based on the size and quantity of edges and surfaces of the aggregates: blocky (Fig. 4a), polyhedral (Fig. 4b), and finely polyhedral (Fig. 4c). Blocky structure aggregates are characterized by their four plane faces, while polyhedral and finely polyhedral structure aggregates typically have more than six. Class II soils are moderately permeable and are commonly found in illimerized B horizons.

A) Blocky B) Polyhedral C) Finely polyhedral

Fig. 4: Types of soil structures within class II (Tomášek, 2007)

Class III. aggregates are rectangular and elongated along the vertical axis. Within this class, structures are distinguished based on the shape of their bases: the columnar structure (Fig. 5a) aggregate has a rounded base, while the prismatic structure (Fig. 5b) aggregate has a flat, polygonal base. Similarly to class III soils, prismatic aggregates within the third class are also moderately permeable and often found in illimerized B horizons.

A) Columnar B) Prismatic

Fig. 5: Types of soil structures within class III (Tomášek, 2007)

Class IV. aggregates are elongated along the horizontal axis. Based on the height of the aggregates, the structures within the class are categorized as: tabular (Fig. 6a) and platy (Fig. 6b). The platy structures of class IV aggregates often overlap, making them the least porous and thereby least permeable. They are commonly found in compacted soils, especially in the eluvial horizons of forest soils (refer to section 3.1.3) (Tomášek, 2007; Pavlásek and Jačka, 2014).

A) Tabular

B) Platy

Fig. 6: Types of soil structures within class IV (Tomášek, 2007)

The presence, dimensions, stability, quality, and special arrangement of soil aggregates determine a variety of physical characteristics of the soil. Structured soils exhibit better water regimes, greater aeration, and easier gas diffusion, than non-structural soils. They also differ in permeability; as mentioned in section 3.2.3, the size and spatial arrangement of soil aggregates and interped spaces impact the porosity as well as pore size. As such, non-structural soils, such as sand, allow for the rapid infiltration of water, while structural soils have aggregates that slow the drainage of water and have a greater water retention capacity. Aside from physical properties, soil structure influences soil erosion resistance, plant growth, and the activity and diversity of soil microorganisms and mesofauna (Kutílek, 1978; Chotte, 2005).

Due to the dynamic nature of soil structure, various methods and soil melioration strategies are used to maintain optimal soil properties and stabilize soil structure, thereby inhibiting the formation of pseudo-aggregates. Such methods include soil liming, tillage, the implementation of crop rotation, and regular application of organic materials (Pavlásek and Jačka, 2014). Synthetic stabilizers from the group of polyacrylates and vinyl acetates are also implemented in soil stabilization (Šarapatka, 2014).

3.2.5. Particle size distribution

Particle size distribution, sometimes referred to as granulometric composition or soil texture, describes the composition of variously sized discrete mineral particles, which are categorized into groups called particle size fractions (Pavlásek and Jačka, 2014; Weil and Brady, 2016).

Particle size fractions

The predefined thresholds of individual particles size fractions vary depending on the used classification system. Typically, they are chosen to ensure that particles within a given fraction exhibit consistent physical or physicochemical properties. In the Czech Republic, the specific thresholds are defined by the Taxonomic Classification System for Czech Soils, which is based on the globally utilized methodology of the United State Department of Agriculture (Kutílek et al., 2004; Pavlásek and Jačka, 2014).

In accordance with the Taxonomic Classification of Czech Soils, soil particles can be divided into two fundamental fractions: skeletal grains (particles > 2 mm) and fine earth (particles < 2 mm). The two-millimeter threshold separating the skeletal grain and fine earth fractions represents a critical point that terminates the impact of capillary forces (Pavlásek and Jačka, 2014).

The skeletal grain fraction consists of particles larger than 2 mm, which can be further classified into the following categories as detailed in Table 3:

Table 3: The classification of the skeletal grain fraction according to the Taxonomic Classification System for Czech Soils (Němeček et al., 2002)

Particle size fraction	Particle diameter [mm]
Coarse sand	2 - 4
Gravel	4 - 30
Cobble	30 - 300
Boulder	> 300

Fine earth, composed of particles smaller than 2 mm, is used as the starting material for establishing granulometric composition and other physical properties of soil. Its categorization within the Taxonomic Classification System for Czech Soils is detailed in Table 4. The 0.002 mm threshold was established based on the colloidal properties exhibited by particles within the clay fraction (Pavlásek and Jačka, 2014).

Table 4: The classification of the fine earth fraction according to the Taxonomic Classification System of Czech Soils (Němeček et al., 2002)

Particle size fraction	Particle diameter [mm]
Sand	0.05 - 2
Silt	0.002 - 0.05
Clay	< 0.002

The representation and percentual composition of individual soil particle fractions is determined through a granulometric analysis. The results of the analysis can then be presented in tabular form or using a grain size distribution curve, which is plotted on a two-axis graph, where the vertical axis represents the percent of particles smaller than or equal to a specific idealized particle diameter. The horizontal axis of the grain size distribution curve contains a logarithmically scaled idealized particle diameter (Kutílek et al., 2004).

Soil texture based on granulometric composition

The percentual composition of individual fine earth fractions serves as the basis for determining soil textures. To establish the soil texture of a given soil, a triangular diagram of basic soil texture classes is used (Fig. 7). This triangular diagram has three axes; the axis along the base of the triangle shows the percentual composition of sand, while the two sides of the triangle show the percentual composition of clay and silt (Kutílek et al., 2004; Němeček et al., 2002).

Fig. 7: Triangular diagram of the basic soil textural classes (NRCS-USDA, 2006)

In accordance with the Taxonomic soil classification system of the Czech Republic, soils are differentiated based on their percentual composition of sand, silt, and clay fractions. This classification system yields 12 soil textural classes, which can be further grouped into five agronomic categories as shown in Table 5 (Němeček et al., 2002).

Table 5: Soil textural classes along with their respective agronomic categories in accordance with the Taxonomic soil classification system of the Czech Republic (modified from Němeček et al., 2002)

Agronomic category	Textural class
Light	sand (S), loamy sand (LS)
Medium light	sandy loam (SL)
Medium	loam (L), silt loam (SiL), silt (Si)
Heavy	sandy clay loam (SCL), clay loam (CL), silty clay loam (SiCL)
Very heavy	sandy clay (SC), silty clay (SiC), clay (C)

The significance of granulometric composition

The percentual distribution of individual particle size fractions heavily impacts various mechanical, physical, and physiochemical properties of soil (Taubner et al., 2009). Thus, granulometric composition is often used alongside other easily measurable characteristics, such as porosity and organic matter content, as an input parameter in pedotransferic functions. These functions estimate less readily determinable hydraulic soil parameters, such as saturated hydraulic conductivity, water retention capacity, and various soil hydrolimits, including wilting point and field water capacity (Kutílek and Nielsen 1994).

Establishing granulometric composition

The most commonly used methods of determining soil texture include elutriation, sedimentation methods, and sieve analysis (Syvitsky, 1991). The method used to determine the granulometric composition of soil samples from Amálie is further discussed in section 5.3.5.

3.2.6. Soil temperature

The soil temperature regime is a characteristic that influences the rates of physical, chemical, and biochemical processes in soil, including water and nutrient uptake, activity of soil biota, nutrient cycling, and root growth (Šantrůčková et al., 2018; Doran and Smith, 1987; Howe and Smith, 2021). It is dependent on the exchange of radiant, thermal, and latent energy facilitated by the physical properties of the soil profile and its surface, as well as the source of energy, which is almost exclusively solar energy (Al-Kaisi, et al., 2017; Kutílek, 1978; Šantrůčková et al., 2018).

Energy partitioning occurs primarily at the soil surface, where various energy transformations and pathways are established. When solar radiation falls on the surface of soil, part of the energy is absorbed, and part of the energy is reflected. The fraction of solar radiation that a surface reflects is measured by albedo, a thermal property influenced by several key factors including slope, orientation, shading of the surrounding relief, and land use (Al-Kaisi, et al., 2017; Howe and Smith, 2021; Lehnert, 2014; Kutílek, 1978)

Table 6: Mean albedo of surfaces based on land use (modified from Ponce et al., 1997)

Land use	Description	Albedo
Bare ground	Soils, dark, wet to light, dry	0.05 - 0.4
	Dark soil, dry	0.14
	Dark soil, moist	0.08
	Clay	0.20
	Desert loam	0.29 - 0.31
Rangelands	Green grass	0.16 - 0.27
Agricultural lands	Potatoes	0.19
	Barley	0.21 - 0.22
	Maize	0.16 - 0.27
	Beets	0.13 - 0.39
	Orchard	0.15 - 0.20
Forestlands	Bog	0.11 - 0.19
	Coniferous forest	0.05 - 0.15
	Deciduous woodlands	0.10 - 0.20

Table 6 illustrates the impact of land use on albedo. For bare ground with no vegetative cover, albedo is determined by soil color, moisture, and texture. As such, the highest absorption occurs in dark, wet, and uneven soils with a southern slope exposure. Due to their high absorption rate, the surface of such soils heats up faster and subsequently radiates more thermal energy. As a result, soils with lower values of albedo have greater daily temperature amplitudes than light, dry, flat soils. Vegetative cover has a dual role in moderating such temperature extremes; it lowers the absorption rate of the soil surface by impeding the penetration of solar radiation, while simultaneously reducing soil heat losses, essentially acting as a thermal insulator. The insulation properties of vegetative cover also have a profound impact on seasonal temperature amplitudes, wherein dense vegetation with a greater leaf

index keeps the soil cooler in the summer and warmer in the winter (Kutílek 1978; Ponce et al., 1997; Lehnert, 2014).

The soil temperature regime of soils is also dependent on its thermal properties, which include specific heat capacity, thermal conductivity, and thermal diffusivity. Their contingency on fundamental physical soil properties such as bulk density, texture, and volumetric water content is shown in Table 7 (Al-Kaisi, et al., 2017).

Table 7: Thermal properties of soil based on soil type, bulk density, porosity, and volumetric water content (modified from van Wijk and de Vries, 1963)

Soil type	**Porosity** [%]	**Volumetric water content** [%]	**Thermal conductivity** [10^{-3} cal·cm^{-1}·s^{-1}·deg^{-1}]	**Volumetric heat capacity** [cal·cm^{-1}·s^{-1}·deg^{-1}]
Sand	40	0	0.70	0.30
	40	20	4.20	0.50
	40	40	5.20	0.70
Clay	40	0	0.60	0.30
	40	20	2.80	0.50
	40	40	3.80	0.70
Peat	80	0	0.14	0.35
	80	40	0.70	0.75
	80	80	1.20	1.15

As exhibited by Table 7, the heat capacity of soil increases almost linearly with water content, making it dependent on both moisture content and the mineral and organic composition of the soils. As a result, soils with a lower water retention capacity, such as sandy soils, have a higher daily temperature amplitude than clayey soils with a higher retention capacity (Lehnert, 2014). This relationship is further substantiated by the correlation between specific heat and soil moisture. The specific heat of water, or the energy required to heat 1 kg of water by 1°C, is greater than the specific heat of soil minerals. Quartz, for instance, has a specific heat of 0.19 calorie per gram, while water has a specific heat of 1 calorie per gram. As such, soils that retain more water require more energy to heat. This not only has an impact on the daily temperature amplitude, but also plays an important role in seasonal variations. Soils with a higher water retention capacity require more energy to heat up during spring and remain warmer in the winter compared to soils with lower retentive capacities (Howe and Smith, 2021).

Seasonal and diurnal temperature variations can also be seen across different soil horizons. As modelled by Fig. 8, deeper soil horizons take longer to respond to changes in aboveground temperature. Thus, daily temperature fluctuations are only reflected by the uppermost soil horizons, while seasonal changes can be seen in greater depths of the soil profile (Al-Kaisi, et al., 2017; Šantrůčková et al., 2018).

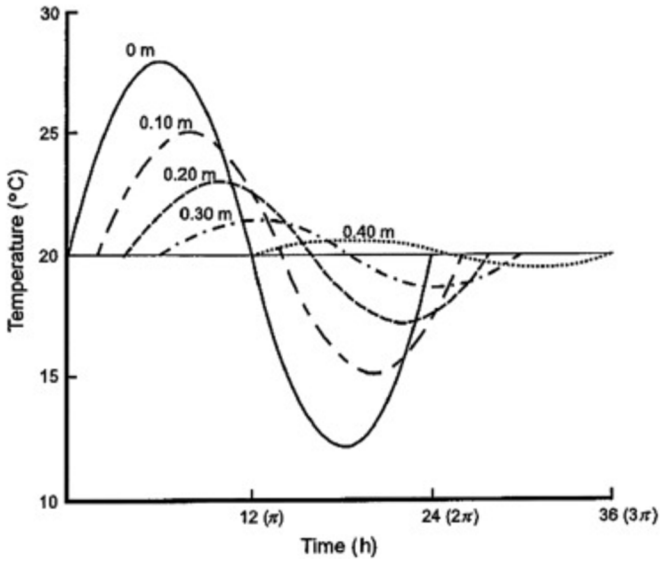

Fig. 8: Temperature fluctuations at different depths of the soil profile (Al-Kaisi, et al., 2017)

Fig. 8 compares the temperature above ground to the temperature in different depths of the soil profile. With increasing depth, the peak temperature response becomes damped and progressively delayed. For instance, at a depth of 0.4 meters, the peak temperature lags approximately 12 hours behind the surface temperature peak and is only about $1/16^{th}$ of the latter (Al-Kaisi, et al., 2017).

Measuring soil temperature

Soil temperature can be assessed using a wide array of methodologies, ranging from soil temperature sensors to remote sensing and satellite monitoring. In Amálie, the temperature regime was monitored using TOMST dataloggers (Fig. 9). TOMST surface dataloggers, which extend to a depth of 14 cm below the ground surface, are equipped with three temperature sensors: T1 measures the temperature at 8 cm beneath the soil surface, while T2 measures the temperature at ground level and T3 measures the temperature at 15 cm above the soil surface. In TOMST dataloggers placed at the depths of 25 cm and 50 cm, both T1 and T2 sensors measure the

temperature at the depth of installation, while the T3 sensor measures the temperature at 15 cm above the soil surface (Wild et al., 2019).

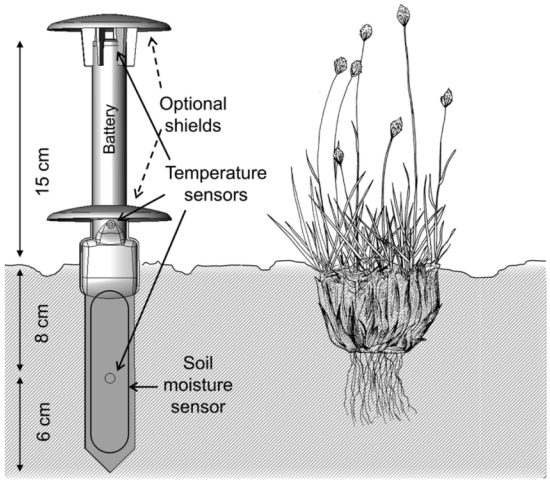

Fig. 9: Temperature and moisture sensors in the TOMST datalogger (Wild et al., 2019)

3.2.7. Soil moisture

Soil moisture is a fundamental quantitative characteristic indicating the total amount of water, including water vapor, in a sample of unsaturated soil. Soil moisture can be expressed both in terms of volume and weight (Kutílek, 1978).

Water content by mass (w), or gravimetric soil moisture, can be determined using the following formula:

$$w = \frac{m_w}{m_M} \quad (5)$$

Where m_w represents the mass of water within a soil sample [g], and m_M is the mass of the solid phase [g]. The mass of the solid phase is determined by the weight of the dried soil sample, which is then subtracted from the total weight of the extracted sample to determine the mass of water (Pavlásek and Jačka, 2014).

Water content by volume (θ) can be expressed using the following formula:

$$\theta = \frac{V_w}{V_s} \quad (6)$$

Where V_w is the volume of water within a soil sample [cm^3], and V_s is the total volume of a soil sample [cm^3]. The resulting value is a dimensionless number constituting

the volumetric water content, which is, at its maximum, equal to the porosity of the soil sample. Although the water content by mass is more accurate, volumetric water content is the preferred method of balancing soil water supply and expressing relative moisture (Kutílek 1978; Pavlásek and Jačka, 2014).

The following equation is used to convert between gravimetric and volumetric expressions of soil moisture:

$$\theta = w\frac{\rho_s}{\rho_w} \quad (7)$$

Where w represents water content by mass, ρ_s is the soil bulk density [g·cm^{-3}], and ρ_w is water density [g·cm^{-3}].

The water contained within soil pores is not always equally available or mobile. Its availability is dependent on a wide range of parameters including the properties of soil particles and their surface (surface area of soil aggregates, surface charge, etc.), characteristics of soil pores (shape, diameter, curvature, etc.), and the properties of the soil solution itself (temperature, density, viscosity, etc.). The most influential parameter, however, is granulometric composition, which directly impacts both the characteristics of soil pores, and the properties of soil particles and their surface. Unlike soil structure, this physical property is inherent and cannot be altered by soil management. As mentioned in sections above, although clayey soils have a higher porosity compared to sandy soils and can retain a higher volume of water, the water they retain is bound by strong forces and is inaccessible to plants. On the other hand, macropore-rich sandy soils exhibit rapid drainage and lower water retention capacity. Loamy soils with a moderately heavy texture exhibit the highest volume of water available to plants (Pavlásek and Jačka, 2014; Saxton et al., 1986; Heitman and White, 2014).

Measuring soil moisture

There are numerous methods for establishing soil moisture, which can be divided into two basic categories: direct and indirect. Direct methods involve the measurement of the amount of water in the soil, while indirect methods determine a physical quantity that is functionally dependent on soil moisture, thereby allowing for the subsequent derivation of water content (Kutílek, 1978).

The standard direct method of determining soil moisture is the **gravimetric method**. In this method, soil moisture is determined by weighing an undisturbed soil, which is then dried and weighed again. The difference in the masses before and after the undisturbed soil sample is dried constitute the mass of the water that was removed from the sample during the drying process (refer to section 5.3.4). Due to its direct nature, the results of the gravimetric method are used as referential values in the calibration of indirect methods of determining soil moisture. Some examples of indirect methods include the resistance, capacitive, gamma ray, neutron, and remote sensing methods (Kutílek 1978; Pokorná and Zábranská, 2008; Šarapatka, 2014). Due to the scope of this thesis, this chapter will only touch on TDT, the indirect capacitive method used to monitor the soil moisture regime in Amálie.

Time-Domain Transmissometry (TDT) measures insertion loss and propagation delay which are reliant on variations in the propagation velocity of transmitted waves (Keysight Technologies, 2023). The TMS dataloggers used to measure soil moisture and temperature in Amálie operate on the basis of the Time-Domain Transmissometry method. In TMS dataloggers, high-frequency (2.5 GHz) electromagnetic pulses are transmitted through a 30 cm circuit shown in Fig. 9. Once a pulse travels through the circuit and reaches the counting unit, another pulse is sent; this is done for 640 microseconds. The number of pulses counted is considered the raw moisture signal and is directly related to soil moisture content. Higher soil moisture yields less pulses. The counts of pulses are then inverted and scaled to the range of 1-4095, with 100 representing ambient air and 3500 representing distilled water. The raw TDT data within this range is then transformed into volumetric water content through a calibration formula (Wild et al., 2019).

3.3. Agroforestry

As the convergence of dry spells and high temperatures occurs more regularly, existing agricultural systems are grappling with the need to adapt to evolving environmental and climatic conditions. In addition to climate change, cropping systems are confronted with a host of challenges related to the soil ecosystem, including moisture and organic matter deficits, nutrient loss, wind and water erosion, compaction, and contamination. The intensification of agriculture has led to the

exacerbation of these problems, making cropping systems less capable of self-regulation and more susceptible to disturbances and environmental changes. To mitigate the risks associated with climate change and prevent further degradation of soil, it is imperative to implement soil amelioration strategies and develop resilient, diversified cropping systems that are better equipped to handle droughts and increased temperatures by effectively regulating the microclimate. Agroforestry serves as a prime example of such amelioration strategies and diversified cropping systems, garnering global attention as a sustainable alternative to conventional agricultural systems (Jacobs et al., 2022; Rolo et al., 2023).

According to Nair (1993), agroforestry systems are defined by two main characteristics. Firstly, there is the intentional cultivation of shrubs or trees alongside agricultural crops and/or animals on the same land unit. The second characteristic necessitates a high level of interaction, either ecological and/or economical, between the woody and non-woody components of the system A simple delineation of agroforestry can be found in Article 23 of the Rural Development Regulation 1305/2013 (Regulation (EU) No. 1305/21013), in which the European Commission defines agroforestry as a land use system where the same plot of land is used for both tree cultivation and agricultural production.

3.3.1. Types of agroforestry

Agroforestry systems in the Czech Republic can be classified into five fundamental categories: silvoarable, silvopastoral, agroforestry in perennial cultures, linear tree plantations at the edges of soil blocks, and urban/rural agroforestry (Lojka et al., 2020).

Silvoarable agroforestry, or agroforestry with cropland, is a system in which linear plantations consisting of woody perennials such as trees and hedges are integrated with crop production, wherein the area allocated for tree cultivation makes up approximately 5-25% of the plot of land (Frelih-Larsen et al., 2022; Lojka et al., 2020). Based on the function and spatial arrangement of trees, the silvoarable agroforestry system can be further divided into two basic groups: linear plantations of forest or fruit trees within soil blocks (alley cropping), and band plantations of fast-growing coppice trees (Lojka et al., 2020).

Silvopastoral agroforestry, also referred to as pasture-based agroforestry, integrates the growth of trees on perennial grasslands with livestock production. This method is predominantly employed for the cultivation of high-statured fruit trees, valuable varieties of deciduous trees, and coppice plantations. The strategic placement of trees, either widely dispersed or planted in clusters throughout the pasture, is designed to optimize the welfare of the livestock (Lojka et al., 2020; Grebner et al., 2022).

Agroforestry in perennial cultures is a traditional system, where the main production is centered around fruit, especially apples, pears, cherries, and plums, within orchards. This is complemented by the secondary production of intercrops or the grazing of livestock, wherein the yield of the secondary production is typically minimal and often fulfilled household needs (Lojka et al., 2020).

Linear tree plantations at the edges of soil blocks, or windbreaks, are a traditional form of agroforestry used to demarcate property by creating boundaries around soil blocks (Janeček, 2008). Currently, these windbreaks, along with hedgerows and tree-lined avenues, serve multiple purposes. They are strategically placed along the edges of soil blocks to mitigate wind and water erosion, segregate soil blocks, and preform additional environmental functions, all while maintaining a productive capacity (Lojka et al., 2020).

Urban and rural agroforestry can be typified by backyard and allotment leisure gardens typically found in rural and suburban regions of the Czech Republic, which combine the cultivation of fruit trees with the production of vegetables, berries, and small domestic animals (Lojka et al., 2020).

3.3.2. Benefits of agroforestry

Agroforestry presents a sustainable approach to agriculture that has the potential to improve soil quality and fertility, prevent soil erosion, enhance water quality and management, conserve biodiversity, regulate microclimate, and mitigate climate change through carbon sequestration (Young, 1997; Jose, 2009; Nuberg et al., 2009; Powlson et al., 2011; Nair and Garrity, 2012). Due to the scope of this thesis, the following chapter will discuss the benefits that pertain to the soil moisture and temperature regime.

The impact of agroforestry on temperature regime

In agroforestry systems, trees regulate the local energy budget, establishing thermal niches by buffering temperature extremes below their canopies. This is achieved through transpiration, a process that transforms water into vapor using energy from the surrounding environment, thereby reducing the amount of sensible heat available for vegetation, soil, and air. The effect of transpiration is further amplified by the ability of trees to decrease radiation flux through the absorption and reflection of solar radiation, as discussed in section 3.2.6 (Jacobs et al., 2022; Richter et al., 2022). Numerous studies pertaining to this phenomenon have observed that the implementation of trees can decrease the average mean temperature of the soil surface, resulting in a lower daily amplitude than in open-field agriculture (e.g. van Noordwijk et al., 2004; Moreno et al., 2007; Karki and Goodman, 2015). This reduction in temperature amplitudes not only protects heat-sensitive crops, but also enhances the performance of various crops such as coffee, cocoa, ginger, and cardamom, as well as cereal crops such as wheat and barley (Rolo et al., 2023; Damatta et al., 2019; Gateau-Rey et al., 2018; Das and Sharangi, 2018; Sharma et al., 2016; Arenas-Corraliza et al., 2018; Inurreta-Aguirre et al., 2018). Reduced average temperatures beneath tree canopies also help to curb excessive transpiration and desiccation of underlying grasses and intercrops. This is particularly evident in Mediterranean woodland pastures, where under the shelter of trees, herbaceous plants and grasses maintain their verdancy for extended periods compared to those in open fields (Rolo et al., 2023; Schoeneberger et al., 2012). Furthermore, the thermal comfort beneath trees in silvopastoral systems has been shown to improve the welfare of livestock (Rolo et al., 2023; Lojka et al., 2020; Galloso-Hernández et al., 2020).

The tree rows in agroforestry systems not only intercept light, but also modulate wind speed, which in turn curtails thermal advection (Baker et al., 2021). Several studies have observed the attenuation of wind velocity at up to 20 times the height of the tree row on the leeward side, and a distance up to 10 times the height of the tree row on the windward side (Baker et al., 2021; Janeček et al., 2008). The porosity of the tree row was also shown to be a critical characteristic, whereby a porosity of 40-60% proved to be most effective. Falling below this range could lead to reduced air pressure on the leeward side, while exceeding it could induce

turbulence (Fig. 10), potentially causing crop damage (Jacobs et al., 2022; Brandle et al., 2004; Cunningham, 1988; Nuberg, 1998; Lawson et al., 2019). Altogether, a properly implemented agroforestry system can significantly influence several microclimatic parameters including temperature, relative humidity, and evaporation (Cleugh, 1998; McVicar et al., 2012). This has been corroborated in a study by Baker et al. (2021), which examined the impact of windbreaks on the microclimatic conditions in paddocks up to 20 tree heights away. This study demonstrated that windbreaks, at peak effectiveness, diminished windspeed by 44%, lowered temperature by 4ºC, and increased relative humidity by 10%. These findings align with those from a study by Bosi et al. (2020), on the microclimatic conditions of a silvopastoral system, and a study by Šinko and Weber (2022) on a silvoarable system. Moreover, reduced wind speed also mitigates mechanical stress and damage to crops, while effectively managing wind erosion (Jacobs et al., 2022).

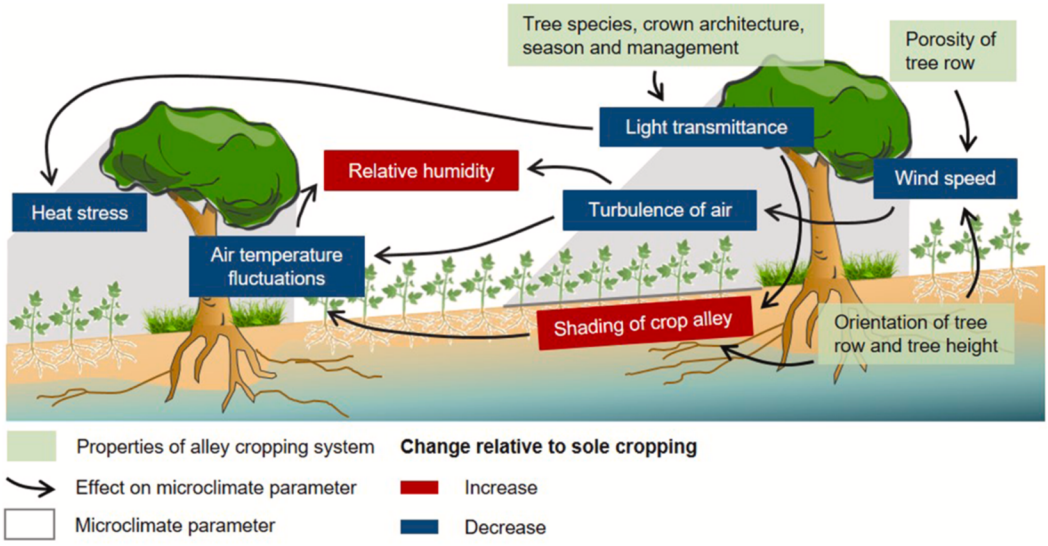

Fig. 10: The impact of agroforestry on microclimate (Jacobs et al., 2022)

Influenced by both wind and air temperature, relative humidity is a pivotal microclimatic parameter that exerts a significant effect on the growth and maturation of crops through its influence on evapotranspiration, water consumption, and crop thermal conditions. According to Bond et al. (2007), vapor pressure deficit rises with increasing air temperature due to the higher moisture-holding capacity of warmer air. This increase of vapor pressure deficit subsequently leads to an elevation in the

transpiration rates of vegetation. This effect was observed in a study conducted by Kanzler et al. (2019), where lower air temperature and vapor pressure deficit was found within forested alleys and their 3m vicinity compared to the crop alley. The vapor pressure deficit in these forested areas was found to be more conducive to plant growth 29% of the time, while instances of water stress due to high vapor pressure deficits were 36% less frequent than in open crop fields. This underscores the potential of agroforestry as a viable strategy for mitigating water stress during periods of heat waves and under conditions of water scarcity (Jacobs et al., 2022).

The impact of agroforestry on soil moisture regime

The soil moisture regime is intricately interconnected with the microclimatic conditions created by agroforestry systems. A decrease in wind speed reduces thermal advection, leading to a decrease in soil evaporation (Vigiak et al., 2003). Reduction in evaporation can also be attributed the lower light transmittance caused by the shading of the tree canopies (Islam et al., 2006; Qi et al., 2011). Furthermore, lower average air and ground temperatures result in a lower transpiration rate, which in turn lead to better water management and lower instances of water stress (Hesslerová et al., 2013). Agroforestry exerts a dual influence on the soil moisture regime, not only through its modulation of the microclimate, but also through its substantial impact on the physical and biochemical properties of the soil ecosystem (Rolo et al., 2023).

Agroforestry modifies the physical and biochemical properties of the soil ecosystem in many ways, one of which is through the production of fresh organic matter (Costa et al., 2017). This process contributes to the formation of the organic litter layer, which not only functions as a soil cover, but also provides microhabitats for epigeic soil organisms. The activity of these organisms facilitates the decomposition and incorporation of organic matter into the topsoil, thereby altering the soil's bulk density and structure (refer to sections 3.2.2, 3.2.4) (Muchane et al., 2020; Ling et al., 2017). Tree roots further stabilize soil structure by interlacing soil aggregates, releasing binding agents such as mucilage and root exudates into the rhizosphere, and enhancing microbial activity (Rolo et al., 2023; Wang et al., 2017). Both tree roots and litterfall influence the composition and activity of soil biota, which in turn affect soil porosity (refer to section 3.2.3), structure and density through

their burrowing activity and fecal deposits (Muchane et al. 2020; Ling et al., 2017; Rolo et al., 2023).

The impact of agroforestry on the physical properties of soil conducive to effective water management has been documented by several studies. A study by Udawatta et al. (2006) revealed that that soils beneath tree buffers possessed 2.4 and 4.7 times more pores than those in perennial grass fields and monoculture crop fields, respectively. Moreover, a notable increase in macropores, and consequently, saturated hydraulic conductivity was observed in the soil under tree buffers, which, according to Cadisch et al. (2004), is conducive to reduced nutrient loss and runoff volume. Extensive research has also been conducted on the bulk densities of soils beneath trees in agroforestry systems. Specifically, Bayala et al. (2014) and Cubera and Moreno (2007) reported lower bulk densities in soils beneath trees of agroforestry parklands and holm oak dehesas, respectively, resulting in higher porosity and infiltration capacity compared to adjacent open fields. Higher porosity, saturated hydraulic conductivity, and infiltration capacity combined with the function of tree alleys as structural elements that can divert and slow down water make agroforestry systems efficient in reducing surface runoff and its erosive force (Spiecker et al., 2009; Jacobs et al., 2022). As shown by Anderson et al. (2006), and Sahin et al. (2016), the combination of these factors causes a faster increase in the soil moisture of forested alleys during recharge periods, potentially leading to higher soil moisture content in tree rows compared to open fields (Spiecker et al., 2009).

The soil moisture regime in agroforestry systems is further impacted by the interplay of interception, throughfall, and stemflow, which determine the partitioning of precipitation between vegetation and soil surface. Interception refers to the process where rainwater is captured by the leaves of vegetation and then evaporated back into the atmosphere. The amount of water intercepted fluctuates temporally and is reliant on leaf area index (Jacobs et al., 2022; Klamerus-Iwan, 2014). The water that the tree canopy cannot hold, along with throughfall - the water that slips through the gaps in the canopy, reaches the soil surface (Jacobs et al., 2022). While interception can decrease the volume of water that permeates the soil, trees generally act as conduits, directing water down their branches and into the ground via stemflow (Johnson and Lehmann, 2006). As noted by van Stan et al. (2016), an optimal arrangement of

canopy structures can enhance stemflow yield and may even promote preferential flow along the roots in the soil.

In agroforestry systems, transpiration is the primary cause of water loss, resulting in increased water usage and subsequently lower soil moisture within tree alleys and their immediate surroundings (Anderson et al., 2009). However, these systems can effectively modulate the microclimate, including wind speed, light transmittance, and air temperature, which has been found to reduce the evapotranspiration rate of nearby open crop fields. A study by Kanzler et al. (2019) found that the potential evapotranspiration in the crop alleys of a coppice agroforestry system was 25% lower than in open fields without interlaid tree rows. While the higher water consumption of trees does increase the risk of competition for water resources, especially during periods of high transpiration rates, a study by Everson et al. (2009) showed that trees forced to develop deeper root systems during periods of drought stress could access water in deeper soil horizons. This highlights the importance of well-designed agroforestry systems, as emphasized by both Jose (2009) and Guo and Zhao (2021), where the different developmental phases of the chosen trees and crops are aligned to avoid competition for water and nutrients. Soil water is also regulated through a process known as hydraulic lift, where tree roots passively move water from deeper, wetter soil layers to shallower, drier ones. The water lifted by the roots at night, when transpiration ceases, is distributed in the topsoil and can be used during the next transpiration period. This hydraulically lifted water provides a daily pool of stored water not only for the trees, but also for more shallow-rooted plants that do not participate in the lifting. During periods of water scarcity, this mechanism can help mitigate the negative effects of soil moisture competition (Allen 2007; Bayala and Prieto 2020; van Noordwijk et al., 2015).

4. CHARACTERISTICS OF THE STUDY AREA

The continuous surveillance of the influence of agroforestry on soil temperature and moisture patterns is currently underway at the Amálie pilot farm, situated in Central Bohemia, approximately 7.6 km east of Rakovník and 41.6 km west of Prague. This farm serves as the experimental site for the Smart Landscape project, an initiative of the Czech University of Life Sciences in Prague, which is dedicated to bolstering existing ecosystems and fostering biodiversity in a cultural landscape that has been adversely impacted by both agricultural and anthropogenic activities.

The study was conducted in a field where an agroforestry system has been implemented. This field is characterized by a sloping terrain with an average inclination of 7% and an elevation of 427m above sea level. Meteorological data for Central Bohemia indicates an average annual temperature of 9.0 °C and an average annual rainfall of 583mm (ČHMÚ, 2023), rendering the area marginally drier and warmer than the national average for the Czech Republic.

The bedrock is composed of shales and graywackes and is predominantly overlayed with haplic eubasic cambisols, with haplic albeluvisols also present in a smaller portion of the area (refer to section 3.1.2) (SPÚ, ©2024; ČGS, 2023). The granulometric composition of the mineral humus horizon (Ah) and the eluvial horizon (E) was similar in all locations, showing an average sand, silt, and clay distribution of 23%-64%-13%, respectively (Fig. 12). Given the substantial percentual composition of silt particles, the soil textural class was identified as silt loam according to the USDA classification.

The study site encompasses a 1.5 ha field, partitioned into three agroforestry alleys each spanning a width of 5 m. In the autumn of 2022, a combination of forest and fruit trees were introduced into these alleys, achieving a planting density of 100 trees per hectare. These agroforestry alleys are interspersed with four strips designated for monocultural crop cultivation (Fig. 11).

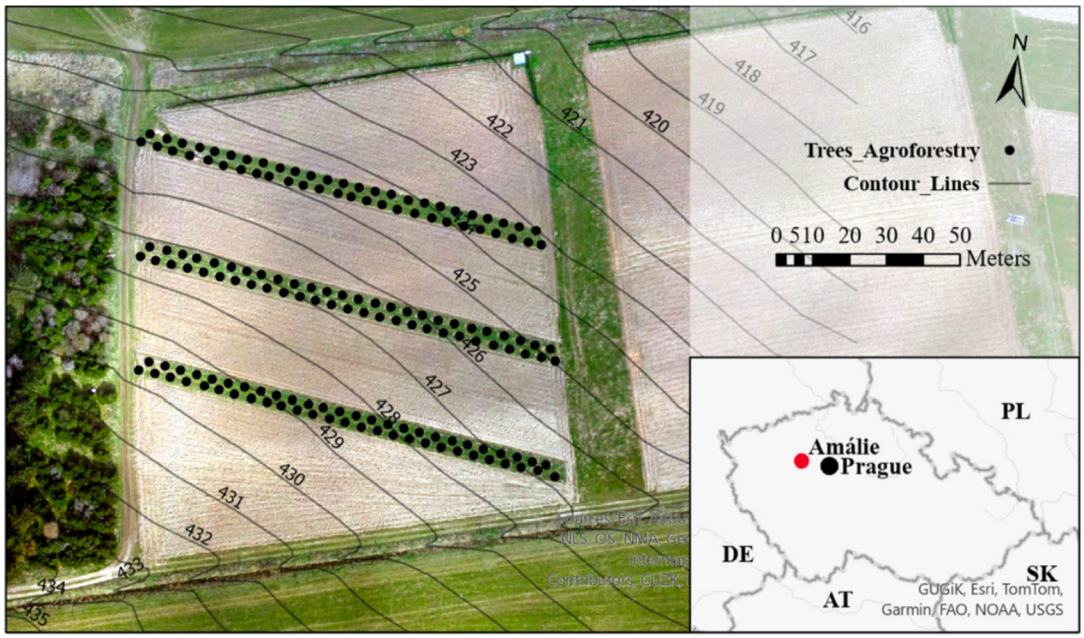

Fig. 11: A map of the studied field with an implemented agroforestry system. The inset map pinpoints the location of the pilot farm, Amálie, in relation to Prague. Black points on the map mark the positions of trees within forested alleys. Altitude is depicted by black contour lines (modified from ČÚZK, ©2010; ČZU, 2022).

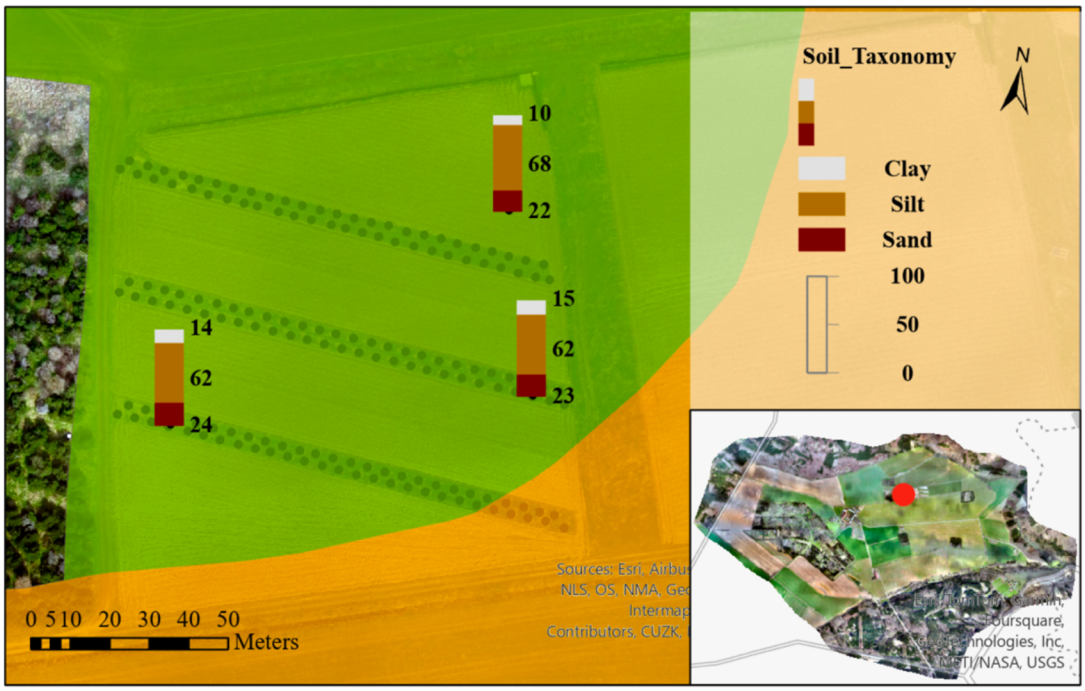

Fig. 12: This map illustrates the distribution of soil types in the area under study. Green-highlighted regions denote areas with Haplic Eubasic Cambisols, while areas marked in orange signify Haplic Albeluvisols. The stacked bars provide a visual representation of the average particle size analysis results for the E horizon at each location. The inset map pinpoints the location of the studied field within the pilot farm, Amálie (modified from SPÚ, ©2024; ČZU, 2022).

5. METHODOLOGY

5.1. Description of the monitoring design

A total of 36 microclimatic stations (TMS TOMST) were placed into three transects perpendicular to the agroforestry alleys and agricultural strips. Their locations are further specified in Fig. 13 and Table 8. The variables measured by the installed TMS sensors are summarized in Table 9. The process and method of standardization, calibration, installation, and the analysis of measured data are further described in section 5.4.

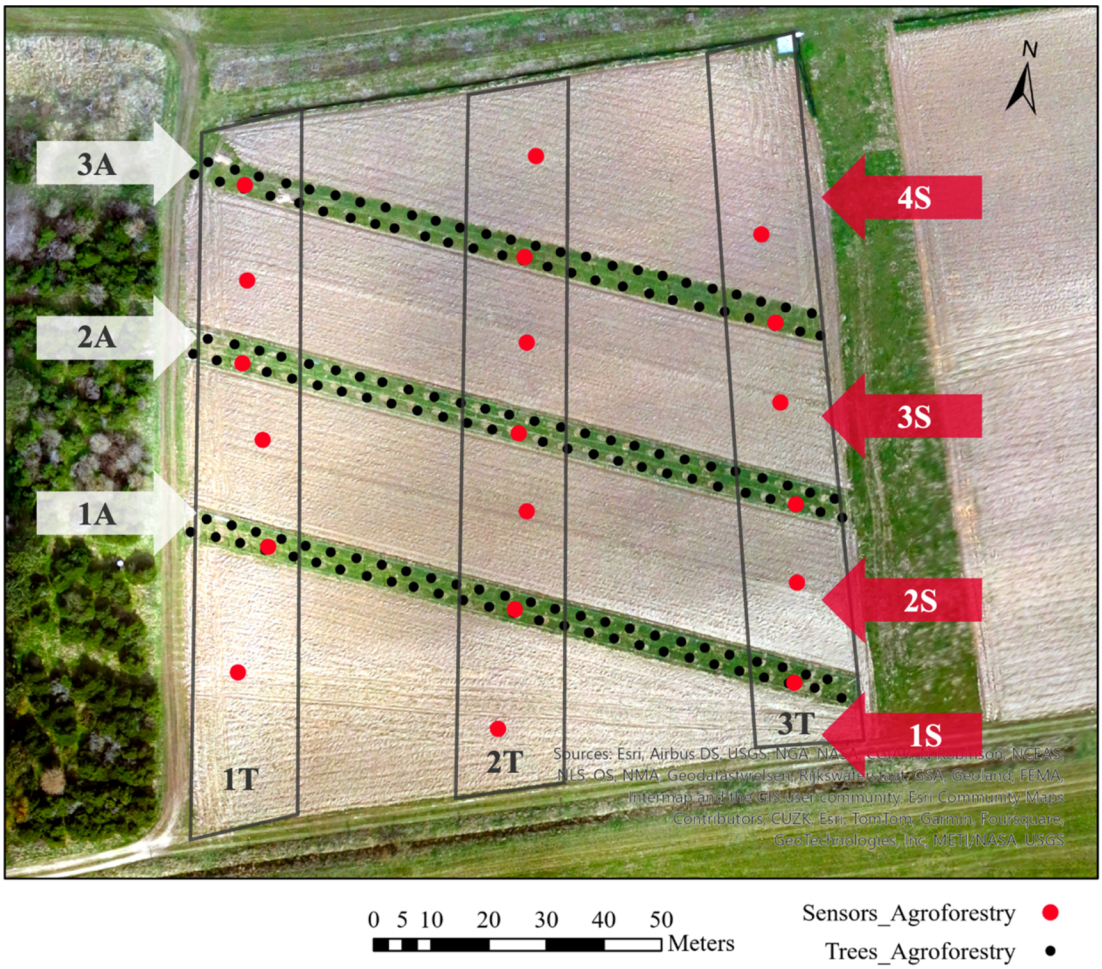

Fig. 13: A map delineating the positions of installed TMS sensors within the studied area. Black points represent trees, while red points represent one or more TMS sensors. The red arrows labelled "S" represent agricultural strips along with their respective numbers. White arrows labelled "A" represent agroforestry alleys with their respective numbers. Boxed areas labelled "T" represent transects perpendicular to the forested alleys and agricultural strips (ČZU, 2022).

Table 8: Specification of the positions and depths of installed TMS sensors

Alley / Strip	Transect	Depth [cm]	Sensor ID
1 A	1 T	14 25 50	041 829 846
1 A	2 T	14 25 50	035 801 805
1 A	3 T	14 25 50	006 804 830
2 A	1 T	14 25 50	049 809 845
2 A	2 T	14 25 50	017 839 837
2 A	3 T	14 25 50	045 836 843
3 A	1 T	14 25 50	022 835 844
3 A	2 T	14	005
3 A	3 T	14	050
1 S	1 T	14	583
1 S	2 T	14 25	529 831
2 S	1 T	14	587
2 S	2 T	14	525
2 S	3 T	14	591
3 S	1 T	14 25	588 817
3 S	2 T	14	528
3 S	3 T	14	590
4 S	2 T	14	584
4 S	3 T	14 25	581 847

Table 9: Variables measured by the installed TMS sensors

Depth of installed TOMST [cm]	**Temperature** (cm above (+)/ below (-) ground)	**Moisture** (cm above (+)/ below (-) ground)
14	(+) 15 0 (-) 8	(-) 8
25	(-) 25	(-) 25
50	(-) 50	(-) 50

5.2. Description of the sampling design

A total of 28 undisturbed samples were extracted from the depths of 8 cm, 25 cm, and 50 cm below the soil surface for the purpose of determining bulk density (5.3.2), porosity (5.3.3), and volumetric water content (5.3.4). The samples were collected on the same days and from the same soil pits that were created in the installation process of the TMS sensors (5.4.2). Once the process of determining bulk density, porosity, and volumetric water content of the extracted undisturbed soil samples was complete, select dried samples were then used to measure particle size distribution 5.3.5. The dates, locations, depths, uses, and corresponding TMS sensors of the extracted sample are documented in Table 10.

Table 10: Specification of the positions, depths, uses, and corresponding TMS sensors of extracted samples

Date of extraction (dd.mm.yyyy)	**Location** (Alley/Strip, Transect)	**Depth** [cm]	**Corresponding TMS sensor**	**Used for particle size distribution** (Yes/No)
16.05.2023	1A, 1T	25	829	Y
		50	846	Y
	1A, 2T	25	801	-
		50	805	-
	1A, 3T	25	804	-
		50	830	-
14.06.2023	2A, 1T	25	809	-
		50	845	-
	2A, 2T	25	839	-
		50	837	-
	2A, 3T	25	836	Y
		50	843	Y
19.06.2023	3A, 1T	8	022	-
		25	835	-
	3A, 2T	8	005	-
		25	-	-
	3A, 3T	8	050	-
	1S, 2T	8	529	-
		25	831	-
	3S, 1T	8	588	-
		25	817	-
	4S, 3T	8	581	-
		25	847	Y

5.3. Physical characteristics of studied soil

5.3.1. Collecting undisturbed soil samples

Upon establishing the site at which the soil sample was to be taken, the area was cleared to ensure that the surface was sufficiently level, without any organic litter or large protruding rocks that could skew the results. The undisturbed soil was extracted using a soil sampling device (Fig. 14) comprised of a standardized stainless-steel cylinder with a length of 4,06 cm and volume of 100 cm^3, which was inserted into a sampling head. This device was then driven into the cleared area of soil with a mallet until the extracted soil column surpassed the upper edge of the cylinder by approximately 0,5-1 cm (indicated by a line on the sampling head. Subsequently, a knife or shovel was used to carefully separate the device from the surrounding soil. After detaching the surrounding soil, a shovel or trowel was used to scoop up the device a few centimeters below its lower edge. The protruding soil was then carefully trimmed off from the center of the cylinder to its edge, into a cone shape, gradually reducing its height until aligned with the cylinder's edge (Fig. 15). Once leveled with the edge of the cylinder, this side of the soil sample was closed off with a plastic cap. The cylinder was then gently taken out of the soil sampling head and the same process was repeated on the upper edge.

Fig. 14: Soil sampling device driven into the soil profile

Fig. 15: Trimming of the soil sample until level with the edge of the sampling cylinder

5.3.2. Bulk density

After acquiring an undisturbed soil sample, the soil was weighed on a precision scale. Subsequently, the plastic caps encasing the sample were removed, weighed, and the sample contained within the stainless-steel cylinder was placed on top of a glass plate of known mass. Together with the glass plate, the sample was then placed into an oven for 72 hours at 60°C to remove any water within the soil. After 72 hours, the sample was removed from the oven and weighed again. Once the mass of the dried sample was established, the sampling cylinder was emptied of the soil and weighed. The bulk density (ρ_s) was then determined using the following equation:

$$\rho_s = \frac{m_d - m_g - m_c}{V_c} \quad (8)$$

Where m_d represents the mass of the soil sample within the stainless-steel cylinder, atop the glass plate [g], m_g is the mass of the glass plate [g], m_c is the mass of the empty sampling cylinder [g], and V_c is the known volume of the standardized sampling cylinder (100 cm^3). The resulting value of soil bulk density is in $g \cdot cm^{-3}$.

5.3.3. Porosity

Soil porosity (P) was measured from the same soil sample as bulk density using the following equation:

$$P = \frac{\rho_M - \rho_s}{\rho_M} = 1 - \frac{\rho_s}{\rho_M} \quad (9)$$

Where ρ_M represents particle density, which is dependent on the mineralogical composition of the soil and is often estimated to be 2.65 $g \cdot cm^{-3}$ due to the high concentration of quartz in most soils. ρ_s is the bulk density of the soil sample [$g \cdot cm^{-3}$], which was measured in the previous step (refer to section 5.3.2).

5.3.4. Volumetric water content

The volumetric water content (θ) was also measured from the same soil sample as bulk density. The first step was to establish the volume of the water (V_w) contained within the sample. Assuming a water density of 1.0 $g \cdot cm^{-3}$, one gram of water is equivalent to 1.0 cm^3. As such, the volume of the water within the soil is equal to the

difference of the mass of the collected sample and the mass of the dried sample, which can be expressed as the following:

$$V_w = (m_w - m_p - m_c) - (m_d - m_g - m_c) \quad (10)$$

Where m_w represents the mass of the collected sample [g], m_p is the mass of the two plastic caps encasing the sample within the cylinder [g], m_c is the mass of the sampling cylinder [g], m_d is the mass of the dried sample [g], and m_g is the mass of the glass plate [g].

Once the volume of water was determined, the volumetric water content (θ) was calculated using the following equation:

$$\theta = \frac{V_w}{V_c} \quad (11)$$

Where V_w represents the volume of water [cm^3] calculated in the previous step, and V_c is the known volume of the standardized sampling cylinder (100 cm^3). The resulting value is a dimensionless number constituting the volumetric water content.

5.3.5. Particle size distribution

Sample preparation

After establishing bulk density, porosity, and volumetric water content, dried soil samples removed from the sampling cylinder were used to determine granulometric composition. First, the desiccated aggregates within the soil samples were broken down with a mortar and sieved through a mesh with a diameter of 2 mm (Fig. 16) to separate the fine soil fraction (clay, silt, and sand) from the skeletal grain fraction (particles over 2 mm in diameter). The remaining clusters of fine soil particles were then broken down chemically and mechanically in a solution of $(NaPO_3)_n$ with a mass concentration of 43.65 $g \cdot l^{-1}$, in which the sample was mixed at a ratio of 1.0ml of the dispersing agent per 1.0 g of soil sample. This is an essential part of the particle size analysis process because it eliminates aggregates formed due to the colloidal properties of the solid phase. The resulting suspension was then diluted with demineralized water to a volume of 200ml and left undisturbed for 24 hours. After 24 hours, the sample was boiled and stirred continuously for 20 minutes, allowing for mechanical dispersion. Following the mechanical dispersion of

aggregates, the sample was cooled in a water bath and wet sieved through a mesh with a 0.25 mm diameter (Fig. 17). The material captured on the sieve was dried in an oven and weighed, while the suspension that passed through the fine mesh was then used to find the granulometric composition of the sampled soil through the hydrometer method.

Fig. 16: Desiccated aggregates being broken down with a mortar and sieved through a mesh with a diameter of 2 mm

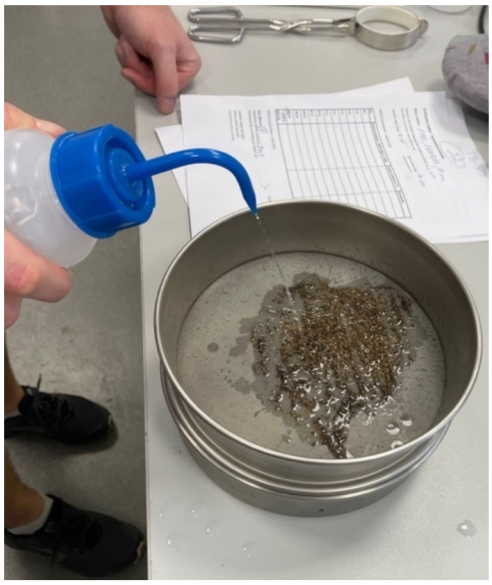

Fig. 17: Wet sieving through a 0.25 mm mesh after the process of mechanical dispersion

Measuring particle size distribution using the hydrometer method

The suspension of fine soil particles that passed through a mesh with a 0.25 mm diameter in the sample preparation process was transferred to a graduated cylinder, where it was diluted to a volume of 1000ml with demineralized water (Fig. 18). It was then vigorously mixed to achieve the complete homogenization of the suspension. As soon as the process of mixing was complete, the timer was started, and the solution's density was recorded 0.5, 1, 2, 3, 4, 5, 15, 45, 120, 150, 320, and approximately 1400 minutes (Fig. 19). The temperature of the solution was measured simultaneously with each measurement of density, with the exception of the first five minutes, during which a constant temperature is assumed.

The first step in evaluating the granulometric composition of the soil sample was the calculation of the density of the referential solution (ρ_{ref}), which is determined using the following formula:

$$\rho_{ref} = \frac{a_0+a_1 \cdot t+a_2 \cdot t^2+a_3 \cdot t^3+a_4 \cdot t^4+a_5 \cdot t^5}{1+b \cdot t} \quad (12)$$

Where a_0 is equal to 999.8395 kg·m^{-3}, a_1 is equal to 16.95258 kg·m^{-3} (°C^{-1}), a_2 is equal to -7.990513·10^{-3} kg·m^{-3} (°C^{-2}), a_3 is equal to -4.624176·10^{-5} kg·m^{-3} (°C^{-3}), a_4 is equal to 1.058460·10^{-7} kg·m^{-3} (°C^{-4}), a_5 is equal to -2.810301·10^{-10} kg·m^{-3} (°C^{-3}), b is equal to 0.0168872 °C^{-1}, and t represents the temperature of the solution [°C].

After calculating the density of the referential solution (ρ_{ref}), the effective depth of the hydrometer (h_r) was calculated using the following formula:

$$h_r = \frac{(S-\rho_s)}{S} \cdot L + \frac{h}{2} - \frac{V}{2 \cdot F} \quad (13)$$

Where S represents the S is the number of large divisions on the hydrometer scale [-], ρ_s is the density of the suspension at a given time [kg·m^{-3}], L is the length of the hydrometer scale [m], h is the distance from the neck of the bulb to its tip [m], V is the volume of the bulb [m^3], and F is the cross-sectional area of the hydrometer bulb [m^2]. The resulting value of the effective depth of the hydrometer (h_r) is dimensionless.

Stokes' law was used to determine the equivalent grain diameter, which can be expressed using the following formula:

$$r = \sqrt{\frac{9 \cdot \eta \cdot h_r}{2 \cdot g \cdot (\rho_M - \rho_{ref})}} \quad (14)$$

Where η represents the dynamic viscosity of water [N·m^{-2}·s], h_r is the effective depth of the hydrometer [-], g is the acceleration due to gravity [9.81 m·s^{-1}], ρ_M is the particle density, which is commonly estimated as 2650 kg·m^{-3}, and ρ_{ref} is the density of the referential solution [kg·m^{-3}]. The resulting value of the equivalent grain diameter is in m.

Finally, the percentual composition of particles smaller than the given substitute diameter was calculated using the following formula:

$$N = \frac{100}{m_d} \cdot \frac{\rho_M}{\rho_M - \rho_{ref}} \cdot (\rho_s - \rho_{ref}) \quad (15)$$

Where m_d is the mass of the dry fine soil particles that passed through a mesh with a 0.25 mm diameter [g], ρ_M is the particle density, which is commonly estimated as 2650 kg·m^{-3}, ρ_{ref} is the density of the referential solution [kg·m^{-3}], and ρ_s is the density of the suspension at a given time [kg·m^{-3}]. The resulting N represents the percentage of the mass (m_d) comprised of a soil fraction that is smaller than or equal to the substitute particle diameter [%].

Fig. 18: Graduated cylinder containing fine soil particles being diluted to a volume of 1000ml with demineralized water

Fig. 19: The stabilization of the hydrometer prior to the measurement of solution density

5.4. Monitoring of soil moisture and temperature by TMS stations

5.4.1. Standardization and calibration

Before installing the TMS monitors into the chosen depths of the soil profile, the TMS signals were standardized to ensure their uniformity in identical moisture conditions. To achieve standardization, the Lolly software was used to set TMS dataloggers to measure in one-minute intervals. For the next fifteen minutes after the alteration of the settings, the 36 dataloggers were set out on the table with the moisture sensor (green segment) hanging off the edge to prevent the distortion of

data due to its contact with the surface of the table. After fifteen intervals of measuring in the air, the 36 dataloggers were transferred into buckets filled with dry glass marbles, which mimicked a porous soil environment. The dataloggers were placed upright with ample distance from each other. After fifteen intervals of measuring within the porous environment of dry glass marbles, the dataloggers were tested in a wet porous environment. To do this, the dataloggers were kept in place while distilled water was added to the marbles (Fig. 20). The water was added carefully to prevent the disruption of the marbles, merely filling in the existing pores. Once all the pores were saturated and the water level was high enough to cover all marbles, another fifteen intervals were measured. Finally, the dataloggers were placed in water (Fig. 21). In order to prevent the contact of individual moisture sensors with the walls of the bucket or with other dataloggers placed within the water, a laboratory support stand was used to clamp the dataloggers by their battery packs (white segment). This held the dataloggers in an upright position and allowed for their stable placement in the water with ample distance from other dataloggers in the same bucket. Once in place, another fifteen intervals were measured.

Fig. 20: TMS dataloggers placed in saturated glass marbles during the standardization process

Fig. 21: TMS dataloggers placed in water during the standardization process

5.4.2. Installation

Upon their standardization and calibration, the TMS dataloggers were set back to their standard measuring intervals (15 minutes) and taken to the studied location in Amálie, where they were installed in agricultural strips and agroforestry alleys.

To install the dataloggers, a 60 cm deep soil pit was excavated. After the extraction of soil samples, the installation process could begin.

First, the depth of 50 cm was measured from the upper edge of the soil pit alongside the wall adjacent to the tree and its roots. An x was marked at this depth on an undisturbed surface, away from any holes made in the sample collection process. Next, a solid metal tool in the shape of the TMS moisture monitor was aligned with the marked x and driven into the soil profile using a mallet. This was done to aid in the insertion of the TMS datalogger and forgo any potential damage that might occur from forcefully wedging it into the soil profile. The metal tool was driven into the soil, aligning the flat moisture sensor segment perpendicular to the upper edge of the soil pit (Fig. 22). This positioning prevents water from pooling on top of the sensor, which could affect the accuracy of the measurements. Given the high contents of clay within the soil, the metal tool was then swiftly removed and replaced with the datalogger before the soil retracted and became impenetrable by the fragile soil moisture sensor. This process involved multiple repetitions until the moisture sensor of the TMS datalogger was fully inserted into the soil profile, revealing only the white segment of the device. After successful insertion, the edges of the inserted segment were coated with damp soil to seal off the moisture sensor and prevent gaps between the device and the soil. This same procedure was then carried out at a depth of 25 cm (Fig. 23).

Once installation was complete, the soil pit was carefully refilled with the removed substrate, ensuring compaction both beneath and above each TMS to maintain stability and prevent damage due to excessive bending. Throughout the refilling process, the TMS datalogger cables were routed alongside the wall of the pit closest to the tree. The top 10 cm of the cables attached to the battery packs and data connectors of the installed dataloggers, remained on the surface, approximately 20 cm away from the tree, and their final stabilization was handled after the installation of the 14 cm TMS.

In a manner similar to the installation of the 25 and 50 cm TMS dataloggers, the insertion of the 14 cm datalogger was preceded by the use of the solid metal tool in the shape of the moisture sensor, which was attached to a driving device and wedged into the soil approximately 20 cm away from the tree, within reach of the aforementioned cables (Fig. 24). The metal tool was then removed and replaced with the soil moisture sensor, revealing only the white segment of the device. After successful insertion, the edges of the inserted segment were coated with damp soil to seal off the moisture sensor and prevent gaps between the device and the soil. Finally, the removable shield for temperature sensor no.3 was attached to the 14 cm TMS.

To secure all three dataloggers in place, the cables of the 25 cm and 50 cm monitors were routed towards the 14 cm datalogger. In agricultural strips that were not protected by a tall fence, the three dataloggers were secured to the sides of the metal cage, which was driven into the ground using a mallet. The metal cage served to protect the dataloggers from wild animals and potential damage from machines, such as string trimmers. In agroforestry alleys protected by high fences, the cables of 25 and 50 cm TMS monitors were secured to a short stake in an upright position (Fig. 25). Finally, the removable shield for temperature sensor no. 3 was attached to the 25 cm and 50 cm TMS monitors.

Fig. 22: Metal tool being placed into the soil profile with the flat segment perpendicular to the upper edge of the soil pit

Fig. 23: Installed 25 cm and 50 cm TMS monitors

Fig. 24: Metal tool being wedged into the soil with a driving device

Fig. 25: Completed installation of the 14 cm, 25 cm, and 50 cm TMS monitors in the agroforestry alley

5.4.3. Collection and analysis of measured data

The TMS microclimatic station data was collected using a touch probe, which was attached to the connector located beneath the removable shield for temperature sensor no. 3. Once a connection was established, the data from the connector was uploaded to a computer with Lolly software, from where the collected data could be exported.

Once exported, the R software environment was then used to process the temperature and soil moisture data collected from all microclimatic stations, removing any data logs before their installation. The data was subsequently categorized according to the measured variable (Table 9) and the location of the TMS, whether in forested alleys or agricultural strips.

Daily maximum, minimum, and mean temperatures were computed for each station. These were then graphically represented in distinct charts based on the height above or depth below the soil surface where the temperature readings were taken. To visually compare the temperature data based on the location of the TMS, the charts featured bold lines, each symbolizing the collective average of the aggregated data of all sensors in either forested alleys or agricultural strips. One pair of lines

represented the average of all daily maximum readings, another pair of lines represented the average of all daily mean readings, and the last pair of lines represented the average of all daily minimum readings.

Daily mean soil moisture data was calculated for each station and divided into separate charts based on the depth beneath the soil surface where the readings were taken. Bold lines on these charts represent the average daily readings, facilitating a visual comparison of soil moisture data between forested alleys and agricultural strips. To examine the relationship between soil moisture and rainfall, this data was plotted alongside precipitation data from a nearby meteorological station (data available only until October 2023). For a detailed view of how soil moisture responds to water input, a brief period in July was left unaggregated, displaying readings at 15-minute intervals. The same visual elements were used in these charts as in the temperature graphs discussed earlier, allowing for easy comparison across different variables.

6. RESULTS

6.1. Physical characteristics of studied soil

6.1.1. Bulk density, porosity, and volumetric water content

The extraction of undisturbed soil samples was done in the first alley on 16.5.2023 from the depths of 25 cm and 50 cm below the soil surface.

Table 11: Bulk density, porosity, and volumetric water content measured from undisturbed soil samples extracted on 16.5.2023 from alley 1

Location (Alley, Transect)	**Depth** [cm]	**Soil bulk density** [g cm^{-3}]	**Porosity** [%]	**Volumetric water content** [%]
1A, 1T	25	1.44	45.63	22.68
	50	1.63	38.39	18.40
1A, 2T	25	1.24	53.32	15.82
	50	1.62	38.74	21.32
1A, 3T	25	1.40	47.02	18.35
	50	1.55	41.33	25.86

Table 11 shows an increase in soil bulk density and decrease in porosity with the increasing depth of extraction from the soil profile. In location 1A,1T, the volumetric water content was higher at 25 cm than at 50 cm. The rest of the locations in alley 1, however, show the opposite trend.

The extraction of undisturbed soil samples was done in the second alley on 14.6.2023 from the depths of 25 cm and 50 cm below the soil surface.

Table 12: Bulk density, porosity, and volumetric water content measured from undisturbed soil samples extracted on 14.6.2023 from alley 2

Location (Alley, Transect)	**Depth** [cm]	**Soil bulk density** [g cm^{-3}]	**Porosity** [%]	**Volumetric water content** [%]
2A, 1T	25	1.47	44.55	15.17
	50	1.4	47.19	16.60
2A, 2T	25	1.29	51.14	11.68
	50	1.74	34.27	13.57
2A, 3T	25	1.44	46.10	12.21
	50	1.43	45.77	20.40

Table 12 shows more inconsistent trends in soil bulk density and porosity relative to the depth of extraction from the soil profile. Both the soil bulk density and porosity

indicate a soil texture that is closer to loamy soil. This is also made evident by the granulometric composition, which shows a lower concentration of silt (52%) in alley 2 soil, than in alley 1 soil (59%). The volumetric water content, however, is consistently higher at the depth of 50 cm.

The extraction of undisturbed soil samples was done in the third alley on 19.6.2023 from the depths of 8 cm and 25 cm below the soil surface.

Table 13: Bulk density, porosity, and volumetric water content measured from undisturbed soil samples extracted on 19.6.2023 from alley 3

Location (Alley, Transect)	**Depth** [cm]	**Soil bulk density** [g cm^{-3}]	**Porosity** [%]	**Volumetric water content** [%]
3A, 1T	8	1.33	49.86	11.06
	25	1.32	50.25	8.97
3A, 2T	8	1.43	45.99	9.30
	25	1.35	48.87	8.94
3A, 3T	8	1.41	46.92	9.58

Table 13 further shows inconsistent trends in soil bulk density and porosity relative to the depth of extraction from the soil profile. Both the soil bulk density and porosity correspond to the silt loam soil texture. The volumetric water content decreases with increasing depth, making it higher in 8 cm, than in 25 cm.

The extraction of undisturbed soil samples was done in agricultural strips on 19.6.2023 from a depth of 8 cm and 25 cm below the soil surface.

Table 14: Bulk density, porosity, and volumetric water content measured from undisturbed soil samples extracted on 19.6.2023 from agricultural strips

Location (Strip, Transect)	**Depth** [cm]	**Soil bulk density** [g cm^{-3}]	**Porosity** [%]	**Volumetric water content** [%]
1S, 2T	8	1.41	46.84	21.51
	25	1.69	36.05	24.18
3S,1T	8	1.21	54.33	16.69
	25	1.23	53.45	19.04
4S,3T	8	1.24	53.35	18.28
	25	1.45	45.15	22.53

Table 14 shows a consistent trend of increase of soil bulk density and decrease in porosity with increasing depth of extraction from the soil profile. It also shows higher

volumetric content at 25 cm than at 8 cm, which is opposite of the trend seen in alley 3, where soil moisture was measured at identical depths of the soil profile.

6.1.2. Particle size distribution

Using the hydrometer method, the granulometric composition of the first transect of alley 1 was established for the depths of 8 cm, 25 cm, and 50 cm below the soil surface.

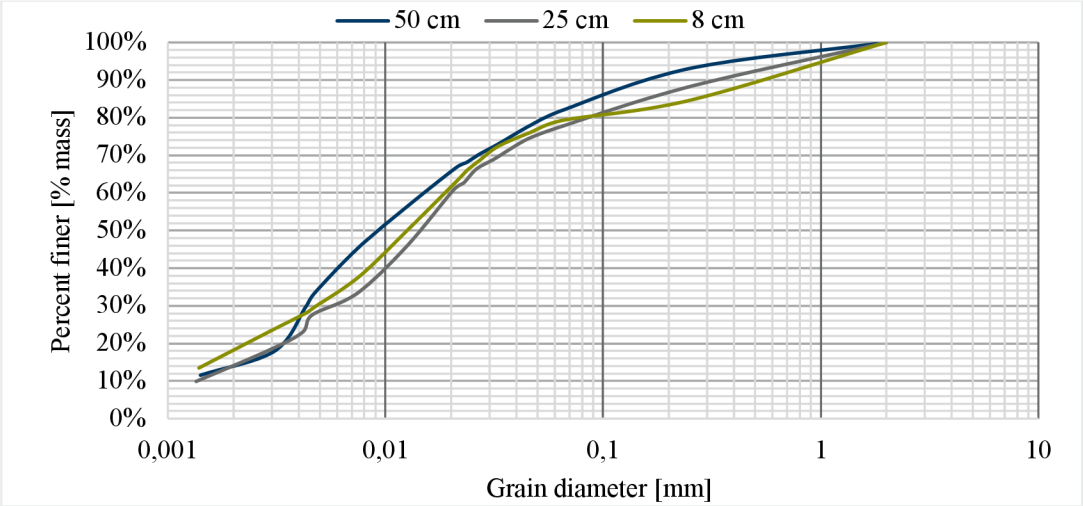

Fig. 26: Grain size distribution curve of 1A,1T

Fig. 26 shows the increase of silt particles with increasing depth. Compared to the 8 cm sample, the 50 cm sample shows a 6 p.p. increase in silt, and a 4 p.p. and 2 p.p. decrease in clay and sand respectively.

The granulometric composition was also found for the third transect of the second alley for the depths of 25 and 50 cm. The results are shown in Fig. 27.

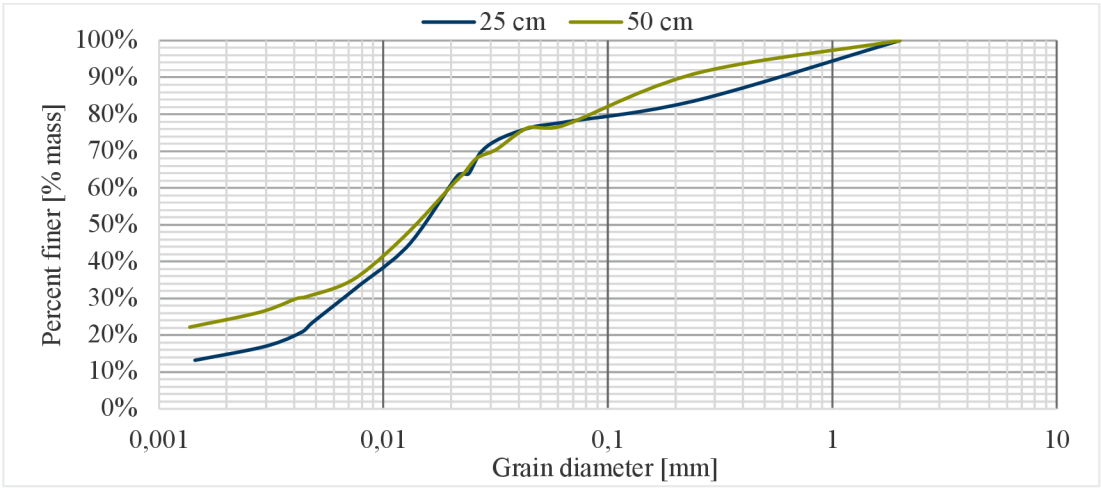

Fig. 27: Grain size distribution curve of 2A,3T

Similarly to the particle distribution of the previously mentioned site, soil samples from 2A,3T have a higher concentration of particles within the 0.002-0.05 mm range. With increasing depth, however, the concentration of silt particles decreases, and the concentration of clay particles increases. This corresponds to the transition into the illuvial and gley horizons of the albeluvisol soil type, which is found near the easternmost positions of the studied alleys.

The last particle size analysis was completed for the third transect of the fourth agricultural strip for the depth of 25 cm. The results are shown in Fig. 28.

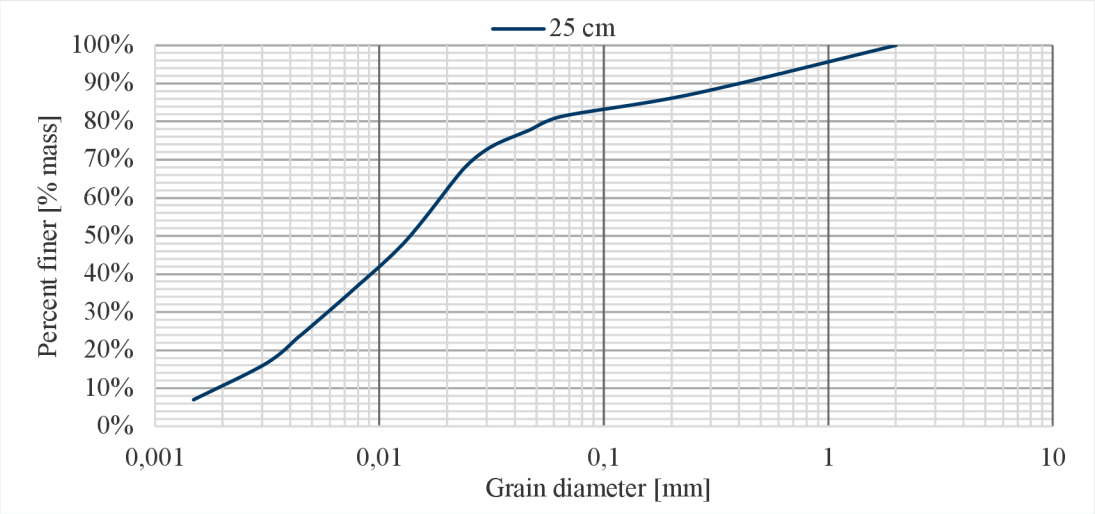

Fig. 28: Grain size distribution curve of 4S,3T

The granulometric composition of the soil found at site 4S,3T contains the highest percentage of silt (68%) found in any of the other tested soil samples. It also has the lowest clay (10%) contents.

A summary of the particle size distribution data can be seen in Table 15:

Table 15: Summarized results of the particle size distribution analysis

Location (Alley/Strip, Transect)	**Depth** [cm]	**Clay** [%]	**Silt** [%]	**Sand** [%]	**Skeletal grain fraction** [%]	**Soil texture**
1A,1T	8	18	59	23	9.64	Silt loam
1A,1T	25	14	62	24	15.98	Silt loam
1A,1T	50	14	65	21	8.44	Silt loam
2A,3T	25	15	62	23	9.63	Silt loam
2A,3T	50	24	52	24	6.35	Silt loam
4A,3T	25	10	68	22	17.45	Silt loam

6.2. Monitoring of temperature by TMS stations

In the following graphs (Fig. 29, Fig. 30, Fig. 31, Fig. 32, Fig. 33), data collected by individual sensors are depicted as translucent, thin lines, while thicker lines illustrate the average readings from these sensors. Temperatures recorded in forested alleys are shown in cool tones: green for daily maximums, blue for daily minimums, and gray for the daily mean temperatures. Temperatures measured in agricultural strips are displayed in warm hues: red for daily maximums, orange for daily minimums, and pink for the daily mean temperatures.

6.2.1. Temperature measured by 14 cm TMS

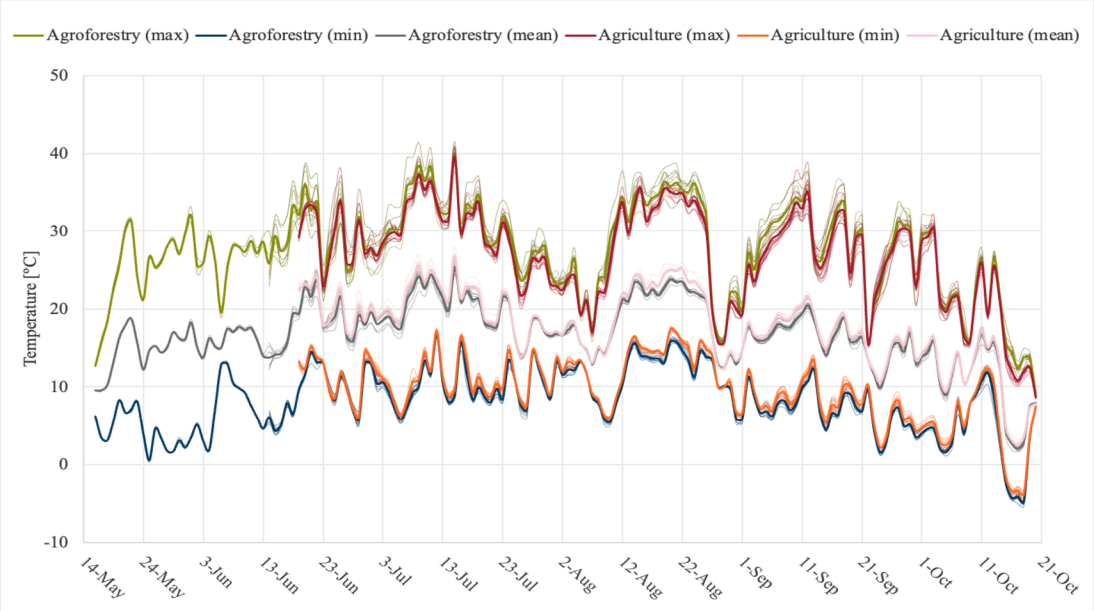

Fig. 29: Aggregated daily temperature maxima, minima, and means measured at 15 cm above the soil surface within agroforestry alleys and agricultural strips

Fig. 29 shows more pronounced temperature fluctuations at 15 cm above the soil surface in forested alleys than in agricultural strips, wherein the maximum temperatures in tree rows are approximately 0.5-1°C higher, while the minimum temperatures are either congruent, or up to 0.5°C lower. Due to the higher temperature maxima and maxima in agricultural strips, the resulting daily mean temperatures are either higher or equivalent to those recorded in forested alleys.

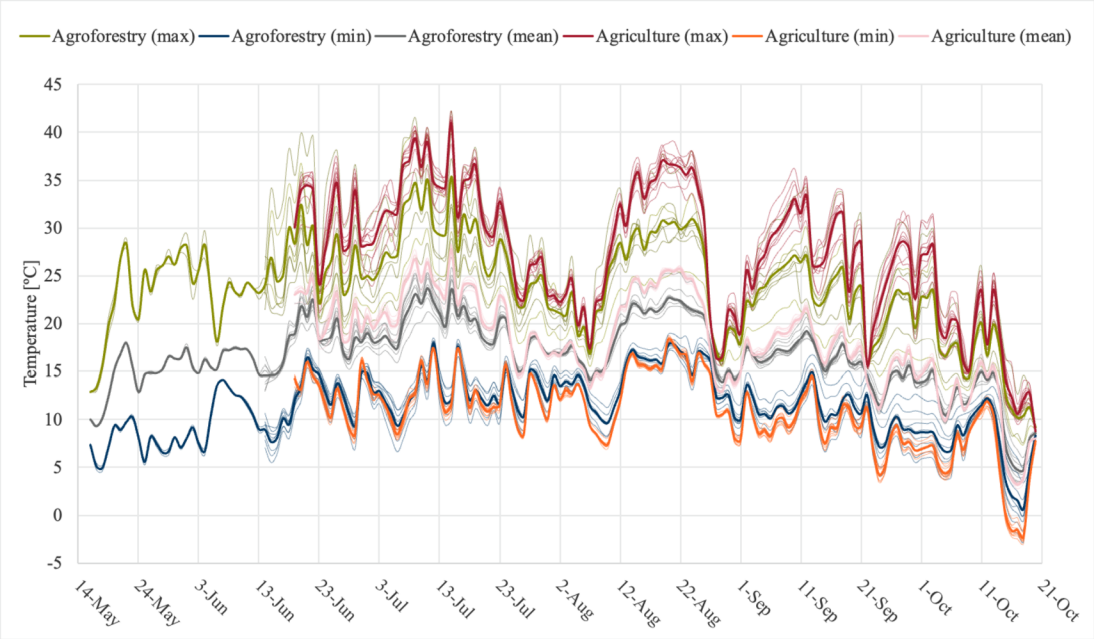

Fig. 30: Aggregated daily temperature maxima, minima, and means measured at the soil surface within agroforestry alleys and agricultural strips

Fig. 30 shows lower temperature amplitudes at the soil surface in forested alleys than in agricultural strips. This is made particularly evident during the August heatwaves, where the temperature maximums in forested alleys were up to 4ºC lower, while temperature minimums were congruent to or slightly higher than those measured in agricultural strips. As a result, the average daily temperatures in forested alleys were consistently lower than those of agricultural strips.

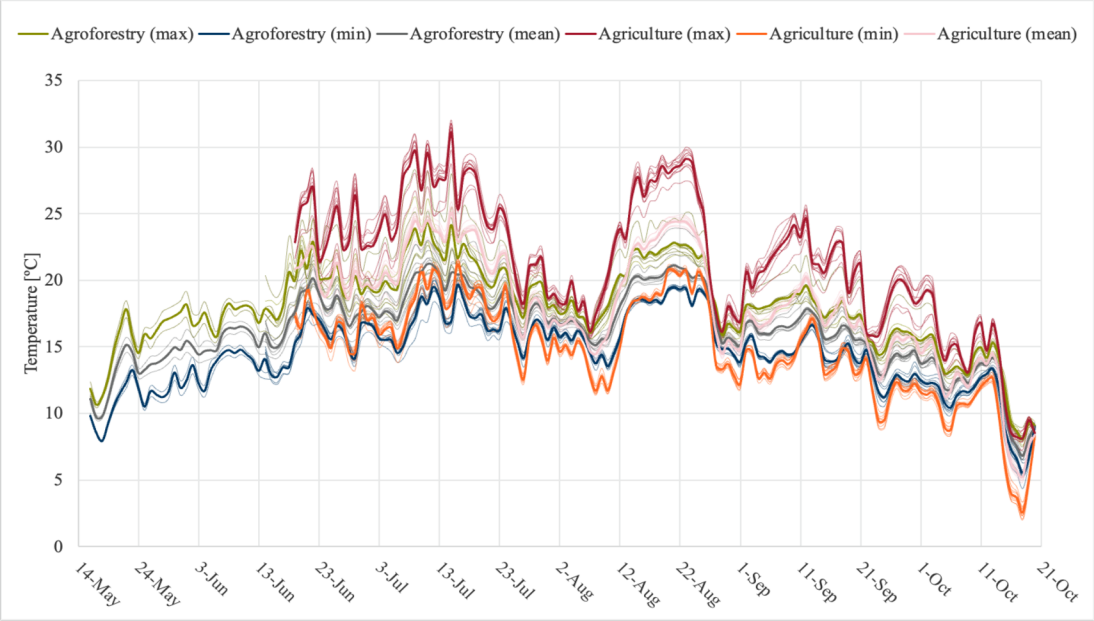

Fig. 31: Aggregated daily temperature maxima, minima, and means measured at 8 cm beneath the soil surface within agroforestry alleys and agricultural strips

Fig. 31 demonstrates a trend similar to that observed at the soil surface, where forested alleys typically exhibit a smaller temperature range and consistently lower average daily temperatures compared to agricultural strips. During the heatwaves in August, the maximum daily temperatures in the rows of trees are even 5°C cooler than those in the agricultural fields.

6.2.2. Temperature measured by 25 cm TMS

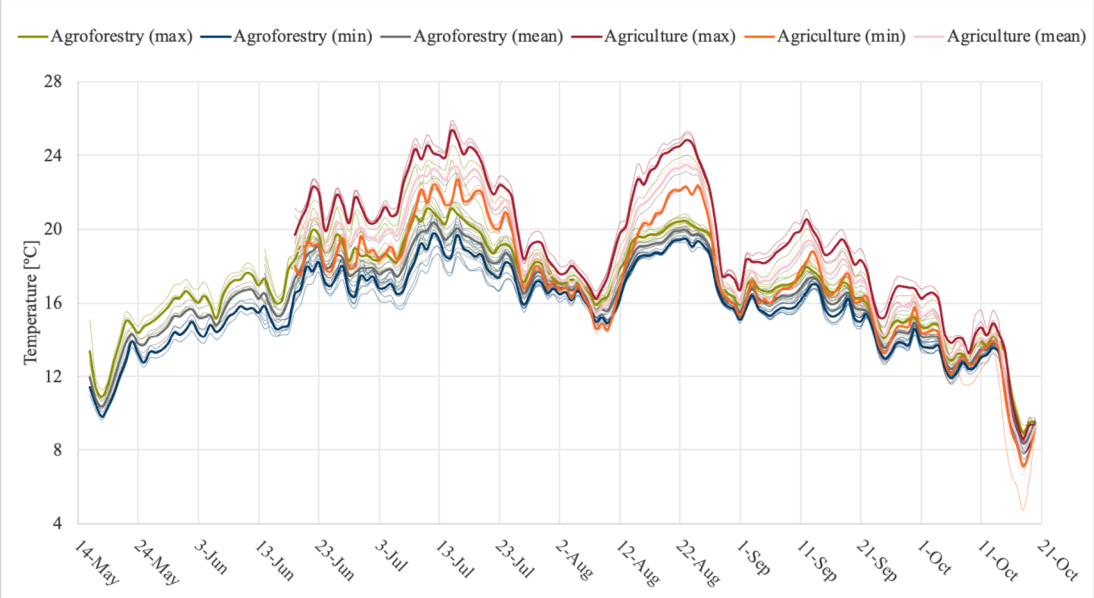

Fig. 32: Aggregated daily temperature maxima, minima, and means measured 25 cm beneath the soil surface within agroforestry alleys and agricultural strips

Fig. 32 illustrates that temperatures 25 cm beneath the soil surface in forested alleys are consistently lower than those in agricultural strips, with the maximum temperatures in the alleys often falling below the minimum temperatures in the agricultural strips. This difference was particularly noticeable during the heatwaves in August, when the soil temperatures in the forested alleys were over 4°C lower than those in the agricultural strips. In general, the temperature variations within the rows of trees are less pronounced.

6.2.3. Temperature measured by 25 cm TMS

As the 50 cm TMS sensors have only been installed in forested alleys so far, the resulting time series solely display their readings without any comparison to a control group.

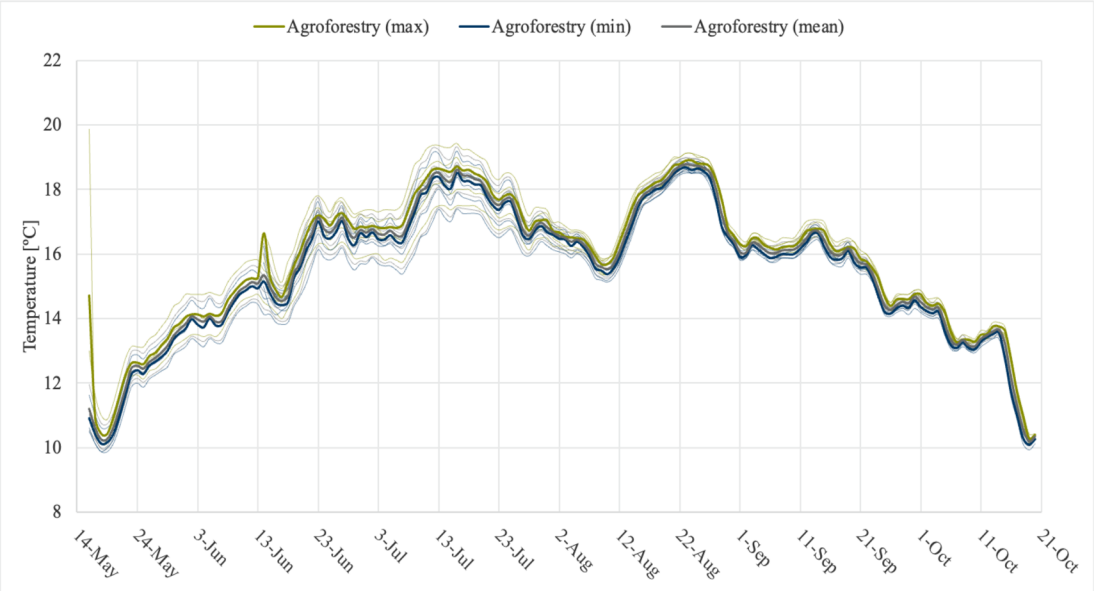

Fig. 33: Aggregated daily temperature maxima, minima, and means measured 50 cm beneath the soil surface within agroforestry alleys

Fig. 33 indicated minimal diurnal temperature variation at 50 cm beneath the soil surface within forested alleys, as evidenced by the small difference between the daily maximum and minimum temperatures. Nonetheless, the impact of the August heatwave is still remarkably evident.

6.3. Monitoring of soil moisture by TMS stations

In the following graphs (Fig. 34, Fig. 35, Fig. 36, Fig. 37, Fig. 38), thin, faint lines illustrate daily average soil moisture recorded by individual sensors in forested alleys (green lines) and agricultural strips (red lines). The bold lines represent the average soil moisture of all sensors within forested alleys (bold green line) and agricultural strips (bold red lines). Precipitation is represented by blue bars, while red bars indicate watering within the agroforestry alleys.

6.3.1. Soil moisture measured by 14 cm TMS

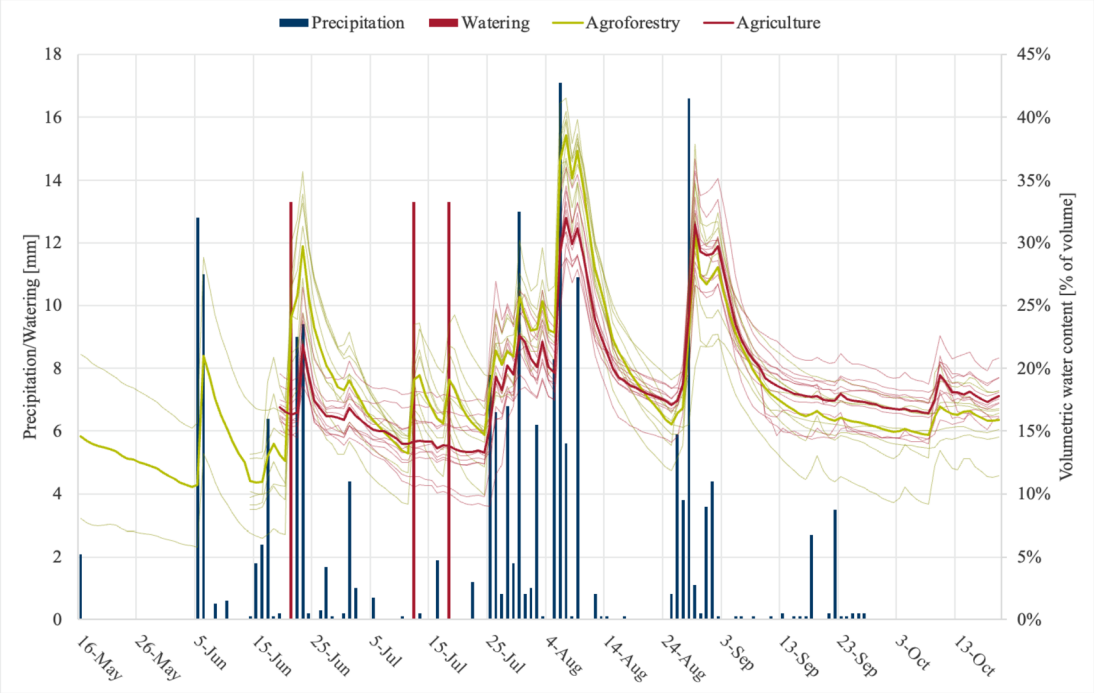

Fig. 34: Aggregated daily mean soil moisture measured 8 cm beneath the soil surface within agroforestry alleys and agricultural strips

Fig. 34 shows that the soil under forested alleys reacts more intensely to heavy rainfall, with an immediate moisture increase of up to 7% more than in agricultural strips. However, the replenished moisture in forested alleys is quickly depleted over the following two weeks, dropping below the moisture levels of the agricultural strips.

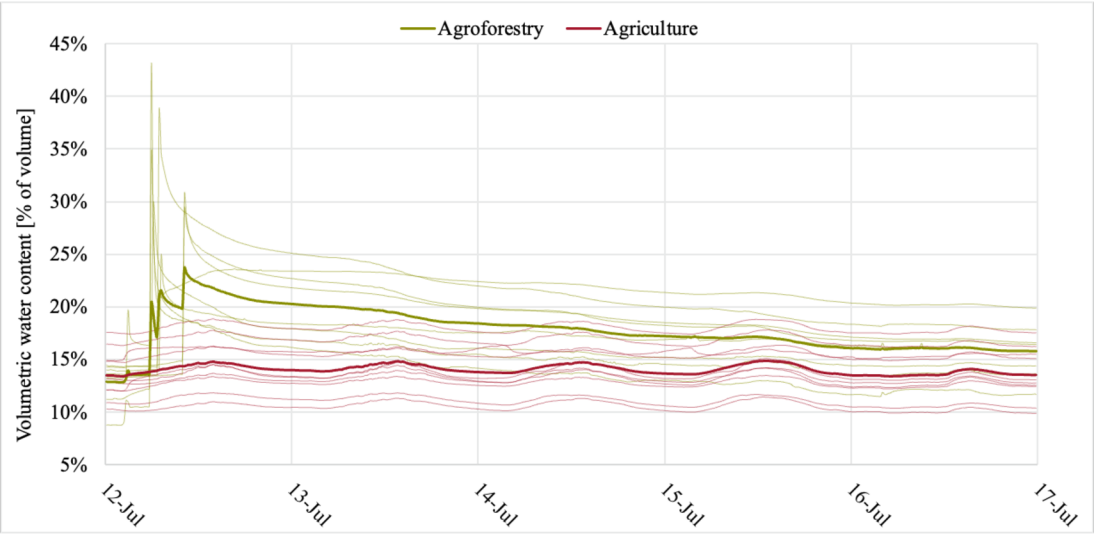

Fig. 35: Non-aggregated soil moisture measured in 15-minute intervals 8 cm beneath the soil surface from 12.7.2023 to 17.7.2023 within agroforestry alleys and agricultural strips

Fig. 35 depicts a rapid increase in soil moisture at 8 cm beneath the soil surface in agroforestry following watering. The soil moisture then decreases by nearly 3% on the first day, 2% on the second day, and 1% each subsequent day in this time series. By the end of the five-day period, the volumetric water content in forested alleys was only 2% higher than in agricultural strips.

6.3.2. Soil moisture measured by 25 cm TMS

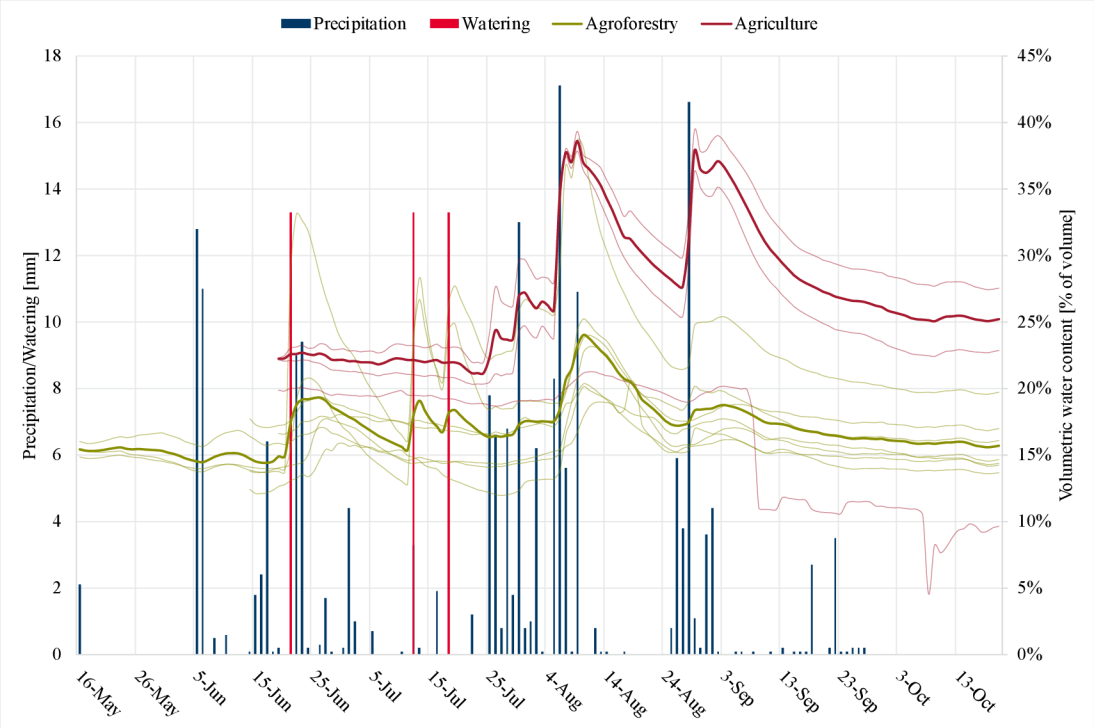

Fig. 36: Aggregated daily mean soil moisture measured 25 cm beneath the soil surface within agroforestry alleys and agricultural strips

Fig. 36 shows consistently lower volumetric water content at 25 cm beneath the soil surface within agroforestry alleys than agricultural strips. Even after receiving 13 mm of watering, the peak soil moisture readings in forested alleys are 3% lower than in untreated agricultural strips. Following a prolonged period of minimal rainfall starting from August 9, 2023, a heavy rainfall event on August 28, 2023, does not significantly affect the soil moisture in the agroforestry alleys. It only shows a slight 2% increase in volumetric water content compared to the lowest soil moisture level recorded since the last major rainfall event on August 9, 2023.

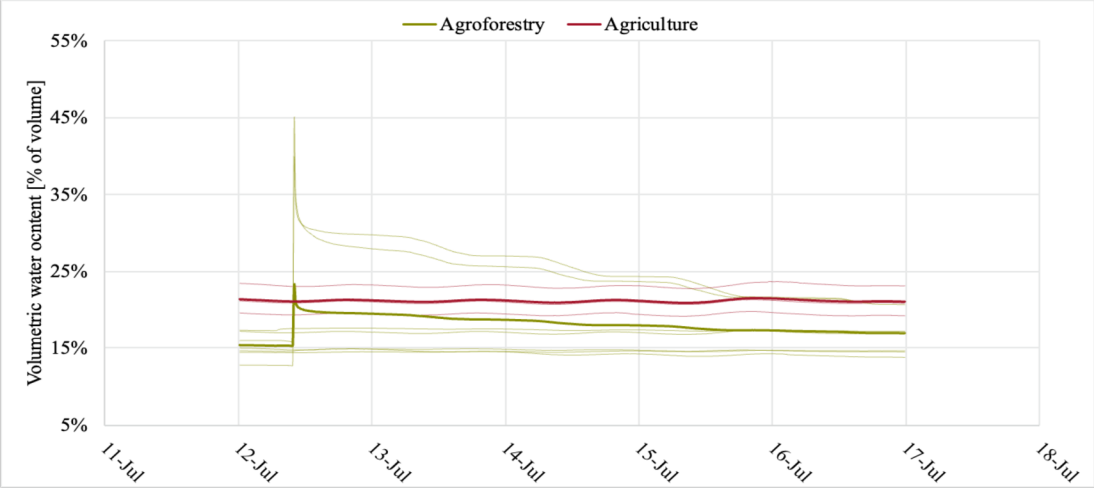

Fig. 37: Non-aggregated soil moisture measured in 15-minute intervals 25 cm beneath the soil surface from 12.7.2023 to 17.7.2023 within agroforestry alleys and agricultural strips

Fig. 37 depicts a rapid 6% increase in soil moisture at 25 cm beneath the soil surface in agroforestry following watering. The soil moisture then decreases by nearly 3% on the first day and continues to decrease by approximately 1% each subsequent day in this time series. By the end of the five-day period, the volumetric water content in forested alleys was 4% lower than that of agricultural strips.

6.3.3. Soil moisture measured by 50 cm TMS

As the 50 cm TMS sensors have only been installed in forested alleys so far, the resulting time series solely display their readings without any comparison to a control group.

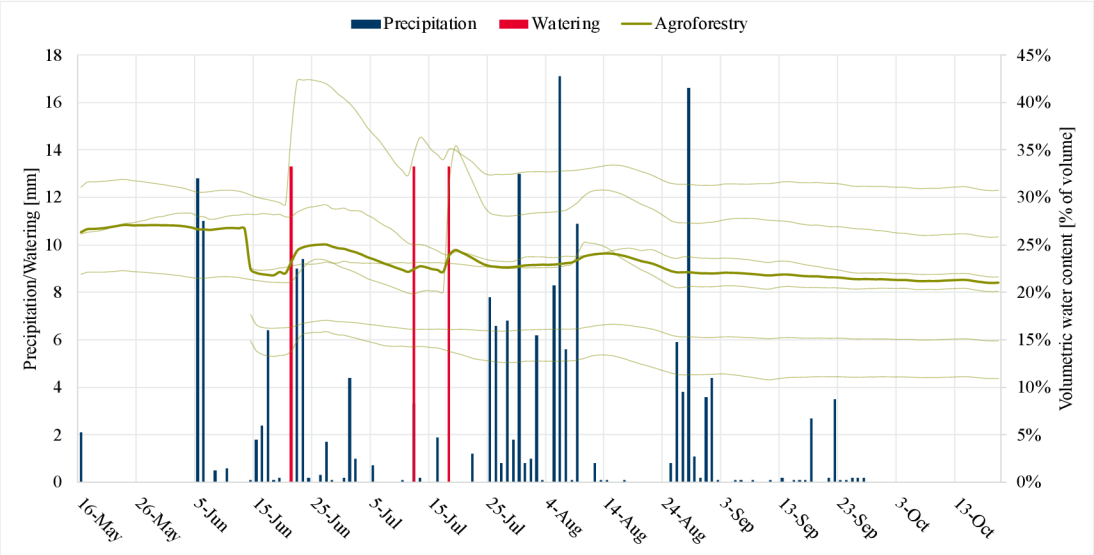

Fig. 38: Aggregated daily mean soil moisture measured 50 cm beneath the soil surface within agroforestry alleys

Fig. 38 shows significant variability in the soil moisture readings of all individual TMS stations. However, all stations exhibit minimal and delayed responses to rainfall and watering. For instance, after a dry spell beginning on August 9, 2023, a substantial precipitation event on August 28, 2023 had no discernable impact on soil moisture levels.

6.4. Comparison of soil moisture measurements

During the installation of TMS microclimatic stations, measurements of the volumetric water content were also done using the gravimetric method. The following graphs (Fig. 39, Fig. 40, Fig. 41) compare the readings of individual TMS sensors, taken a day post-installation, with the soil moisture measurements obtained from undisturbed soil samples at various depths within the soil profile.

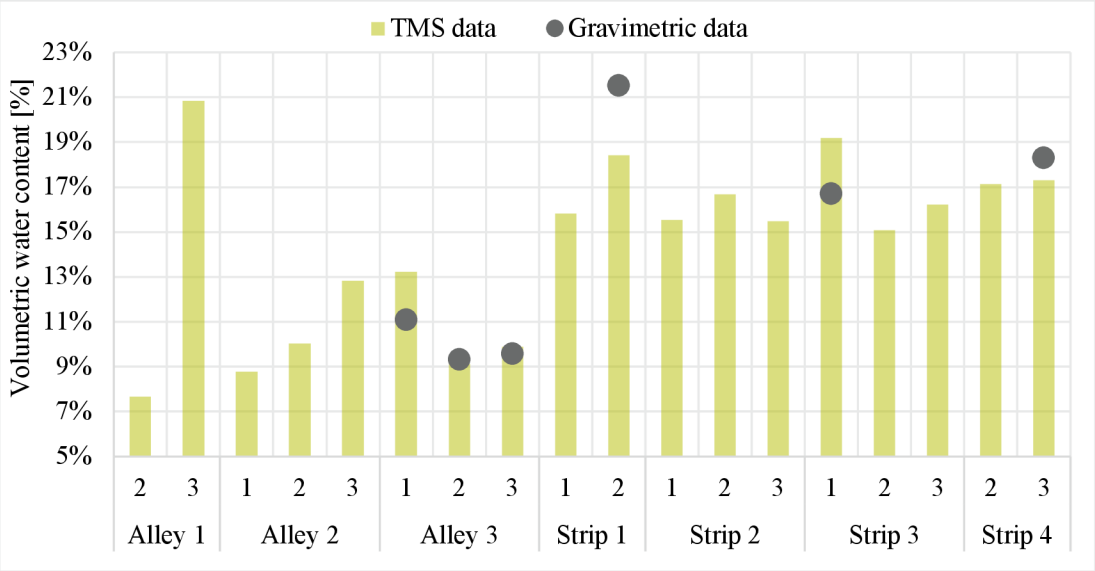

Fig. 39: Comparison of the volumetric water content measured at 8 cm beneath the soil surface by TMS stations and from undisturbed soil samples

Fig. 39 illustrates that the average absolute discrepancy between the volumetric water content readings from the TMS stations and the measurements obtained through the gravimetric method is 1.2%.

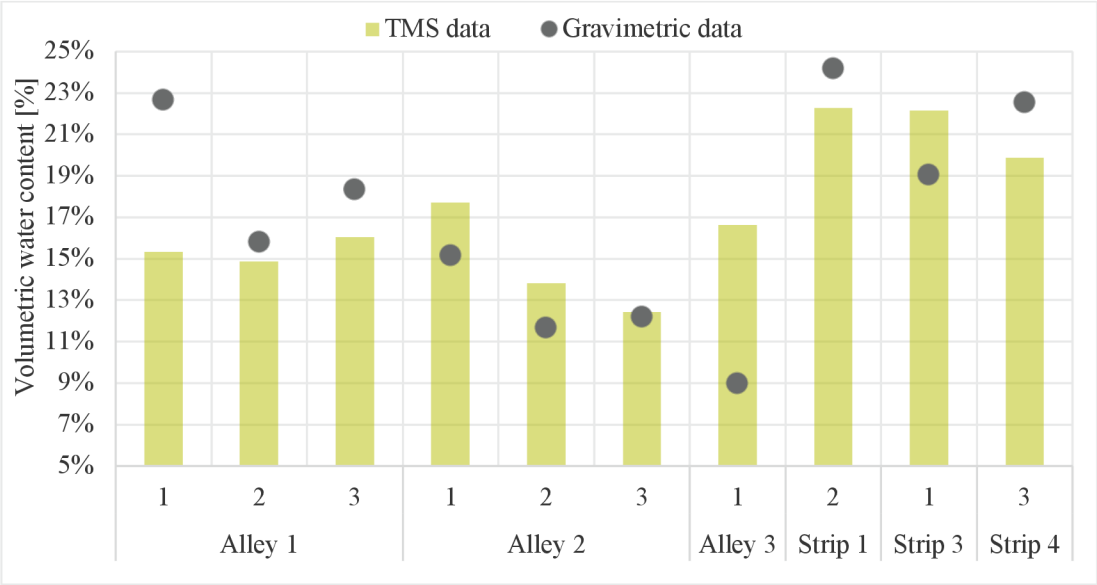

Fig. 40: Comparison of the volumetric water content measured at 25 cm beneath the soil surface by TMS stations and from undisturbed soil samples

Fig. 40 shows an average absolute discrepancy of 3.1% between the volumetric water content readings from the TMS stations and the measurements obtained through the gravimetric method.

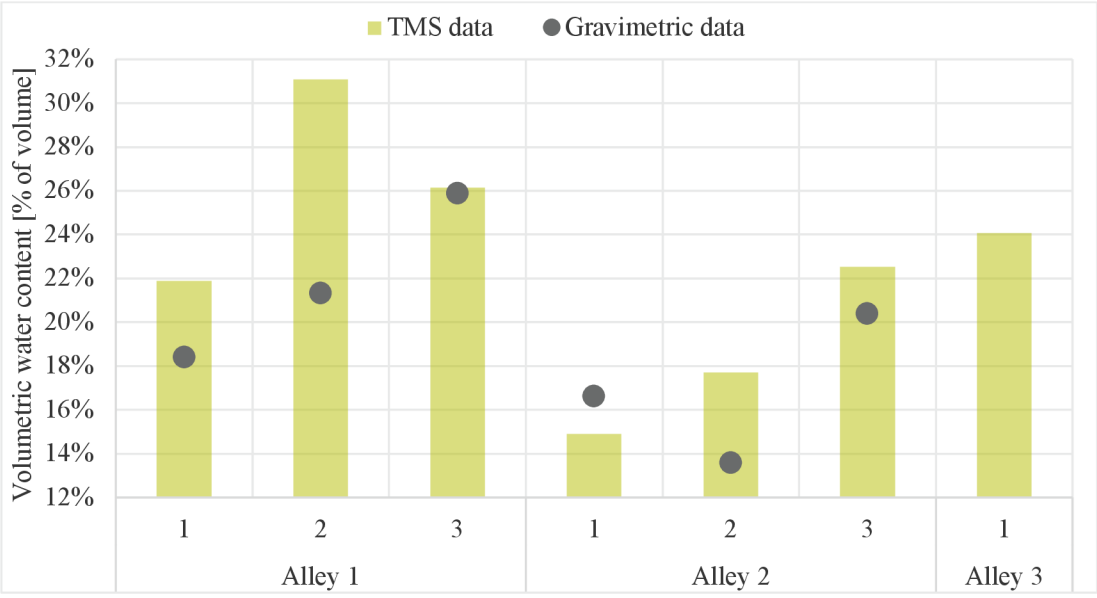

Fig. 41: Comparison of the volumetric water content measured at 50 cm beneath the soil surface by TMS stations and from undisturbed soil samples

Fig. 41 shows an average absolute discrepancy of 3.6% between the volumetric water content readings from the TMS stations and the measurements obtained through the gravimetric method.

7. DISCUSSION

As the convergence of dry spells and high temperatures becomes increasingly frequent across central Europe, existing cropping systems face formidable challenges in adapting to shifting environmental and climatic conditions. The mitigation of risks associated with climate change requires the implementation of more resilient and diversified cropping systems that can effectively withstand droughts and increased temperatures (Beillouin et al., 2020; Sedlmeier et al., 2018; Lüttger and Feike, 2018; Webber et al., 2020; Paul et al., 2017).

According to Gosme et al. (2016) and Martin-Chave et al. (2019), the trees within an agroforestry system play a pivotal role in modulating daily temperature fluctuations by reflecting and absorbing both nightly radiation and daily incoming solar radiation. There are copious studies which have observed the same trend. For instance, Karki and Goodman (2015) examined the microclimatic differences between silvopasture and open pasture systems on the Coastal Plain of Southeast USA. Results of their three-year monitoring revealed that silvopastures had milder microclimatic conditions, with an average temperature approximately 2.1ºC lower than in open pastures. The impact of agroforestry on microclimate is further corroborated in a study by Steffan-Dewenter et al. (2007), which investigated land use strategies within cacao agroforestry systems in Sulawesi, Indonesia. Their findings showed that the removal of shade trees led to a substantial increase in soil surface temperature by about 4ºC. Moreover, reduced diurnal and seasonal temperature fluctuations in agroforestry systems were documented by Moreno et al. (2007) in their study assessing the microclimate in Mediterranean dehesas (Jacobs et al, 2022; Rolo et al, 2023). The results of the temperature monitoring at the Amálie location revealed a lower temperature amplitude both at and below the soil surface of forested alleys, than in agriculture strips, further substantiating the statement made by Gosme et al. (2016) and Martin-Chauve et al. (2019). However, this phenomenon did not arise from the shading effect of tree canopies on the soil surface, which would typically lead to temperature moderation due to reflection and absorption of radiation energy. Given the age of the trees and the respective size of their canopies, this effect was instead attributed to the presence of tall grasses within the agroforestry alleys. Furthermore, the application of highly concentrated herbicides to the sorghum crop within the

agricultural strips resulted in crop damage. This damage led to the absence of vegetative coverage, which in turn, caused inflated temperature amplitudes. As such, the resulting amplitudes do not accurately represent the true conditions within an agricultural strip with a crop monoculture.

While the diurnal temperature amplitudes both at and below the soil surface of forested alleys were lower than those observed in agricultural strips, this pattern did not hold true for temperatures measured 15 cm above the soil surface. Fig. 29 illustrates that within agroforestry alleys, the daily maximum temperatures at 15 cm above the soil surface exceeded those recorded in agricultural strips, while the daily minimums consistently remained equivalent or lower, making the overall daily mean temperature up to 2ºC lower. Despite their higher air temperature amplitudes, forested alleys consistently exhibited lower soil temperature amplitudes. Notably, unlike the bare agricultural strips, which lacked any insulative vegetation cover, the forested alleys of Amálie had maintained dense grasses exceeding 1 meter in height. A similar phenomenon was documented in a study done by Swieter et al. (2021). This study was conducted on a short rotation coppice agroforestry system in Germany, where tree row orientation was nearly perpendicular to the prevailing west/south-west wind direction, representing an analogous slope orientation and prevalent wind direction to those of the Amalie location. The results recorded by Swieter et al. showed lower minimum air temperatures in the morning in forested alleys compared to the referential crop field. However, during the afternoon, the forested alleys experienced higher air temperatures, resulting in greater daily temperature amplitudes. According to Brandle et al. (2004), this phenomenon could be partially attributed to reduced wind speed, which significantly impacts heat transfer and evaporative cooling processes (Jacobs et al, 2022).

Agroforestry systems have a significant impact on the water balance. According to Spiecker et al. (2009), rows of trees with continuous plant coverage serve as a structural feature that can redirect and decelerate water flow. This diminishes the erosive impact of surface runoff and increases infiltration. The impact of agroforestry on reducing surface runoff is further corroborated by a study conducted by Nerlich et al. (2013), wherein the integration of poplar and hardwood timber trees resulted in a 90% decrease in surface water runoff when compared to a monoculture field.

Furthermore, a study done by Kay et al. (2018) showed a 0.5% decrease in the percentage of rainfall lost to surface runoff when comparing farmland to an agroforestry landscape. This effect was also seen in soil moisture regime of forested alleys in Amálie. The placement of trees, perpendicular to the north-south slope orientation, allowed the interlaying forested alleys to infiltrate surface runoff from the bare agricultural strips. This is one of the possible reasons why the 8 cm soil moisture sensors illustrated greater peaks in response to rainfall (Fig. 34).

Several authors, including Van Stan et al. (2016) and Li et al. (1997), have also observed that the appropriate configuration of canopy structures can be conducive to higher stemflow yield and can even stimulate preferential flow within the soil. Although the greater soil moisture peaks in the forested alleys of Amálie following precipitation events cannot be attributed to stemflow due to the early stage of development of the trees, their root systems could have facilitated some preferential flow. Similarly, the dense, tall grasses in forested alleys may have channeled rainwater beneath the soil surface, where it then traveled through the pores around the grass roots. This phenomenon aligns with the findings of Basche and DeLonge (2017), who found that both living and dead tree roots can create channels for preferential water flow.

While it is crucial to recognize the benefits of agroforestry, it is equally important to consider the potential risks associated with the high water uptake by trees and understory vegetation in forested alleys. As noted by Jacobs et al. (2022), trees typically exhibit elevated transpiration rates compared to annual crops, resulting in higher water consumption. This observation is further supported by a study conducted by Petzold et al. (2009), which found that a poplar short rotation coppice agroforestry system consumed significantly more water than winter wheat, primarily due to its longer vegetation period. The higher usage of water by trees and the consequent low volumetric soil content has been reported by several authors, with Caubel et al. (2003), and Sahin et al. (2016) observing low soil moisture in forested alleys particularly during the summer season (Anderson et al., 2009; Reynolds et al., 2007; Jose et al., 2000). A similar trend was observed in agroforestry alleys during the monitoring of soil moisture in Amálie. Although the combined impact of decreased evaporation and surface runoff resulted in a higher volumetric water content 8 cm below the soil surface

during periods of regular rainfall and supplementary watering, the water consumption by trees and understory vegetation surpassed these effects, especially immediately after and during periods of prolonged dry spells. An example of this is when a ten day long dry spell was followed by a significant rainfall event on August 28, 2023. Unlike previous significant rainfall events, which resulted in higher peak soil moisture at 8 cm in forested alleys compared to agricultural strips, the soil moisture peak following this event was 2% lower in the agroforestry alleys. Two weeks after this rainfall event, the volumetric water content at 8 cm in the forested alleys was further reduced by 2% compared to the agricultural strips, likely due to the rapid water consumption by the trees and understory vegetation. At a depth of 25 cm, the response of agroforestry alleys to rainfall was even less pronounced, showing only a minor 2% increase in soil moisture compared to the lowest level recorded since the last major rainfall event on August 9, 2023. At a depth of 50 cm, agroforestry alleys showed no response to the rainfall event, suggesting that the trees and understory vegetation likely absorbed the water before it could reach the lower soil layers. This rapid depletion of water supply could result in soil moisture levels falling beneath the permanent wilting point, leading to tree death or competition with crops in adjacent agricultural strips (Zeitoun et al., 2021). A study conducted by Coussement et al. (2018) in Belgium observed such competition at a distance of 15 meters from a row of mature poplar trees beneath the adjacent agricultural strip. Similar results were found by Mulia and Dupraz (2006), who found poplar tree roots extending more than 8 meters from the tree under a wheat field. However, Upson and Burgess (2013) suggest that younger trees, with roots located in shallower soil layers, are more likely to compete with agricultural crops than mature trees with deeper established root systems. Thus, agroforestry systems with mature trees may have less of an impact on crops in adjacent agricultural strips.

As this study is still in its early stages, it is important to acknowledge the potential limitations and discrepancies in the TMS microclimatic stations as they settle into the soil and establish better contact with the surrounding environment. These discrepancies are particularly evident in the comparison of volumetric water content measured by the gravimetric method and the TMS stations (Fig. 39, Fig. 40, Fig. 41). It is possible that the inconsistent volumetric water content results were caused during the installation process, which was carried out during dry summer months. The soil pit

made during this process may have dried out slightly, making the extraction of soil samples more difficult particularly in deeper soil layers with a higher clay composition and leading to variability in the results. Furthermore, the soil's disruption during the installation process might have prevented the TMS moisture sensors from establishing good contact with the surrounding soil environment. As pointed out by Wild et al. (2019), a loss of contact, especially in soils that shrink and swell, can result in lower than actual soil moisture values. This phenomenon can be seen in Fig. 36 where after an extended dry period, the soil around the TMS station likely contracted, leading to a loss of contact with the moisture sensor and a subsequent decrease in soil moisture readings.

8. CONCLUSION

Agroforestry, a sustainable land use system that combines tree cultivation with agricultural production on the same plot of land, has the potential to improve microclimatic conditions and management of water during periods of dry spells and extreme temperatures brought on by climate change (Jacobs et al., 2022). Throughout the course of this bachelor thesis, 36 TMS microclimatic stations were installed in the forested alleys and agricultural strips of the Amálie location to assess the effect of tree rows on the temperature and soil moisture regime of silt loam soil.

The findings of this study lend credence to the assertion by Gosme et al. (2016) and Martin-Chauve et al. (2019) that trees in an agroforestry system can modulate daily temperature fluctuations by absorbing and reflecting both nocturnal and diurnal solar radiation. This was evident in the data collected from Amálie, which showed that during the August heatwaves, the daily maximum temperatures in the agroforestry alleys were 7ºC lower than those in the agricultural strips. This trend was also observed below the soil surface, at depths of 8 cm and 25 cm, where the peak temperatures were nearly 4ºC lower. However, to corroborate the findings of Moreno et al. (2007) that agroforestry systems can reduce seasonal temperature fluctuations, a more extended period of temperature monitoring would be necessary.

In addition to the observed temperature modulation, it was also found that the temperature at a height of 15 cm above the soil surface in the agroforestry alleys was either comparable to or up to 2ºC higher than that in the agricultural strips. This phenomenon, as explained by Brandle et al. (2004), could be attributed to the reduced wind speed in the agroforestry alleys, which significantly influences heat transfer and evaporative cooling. To further validate this hypothesis, it would be necessary to measure the wind flow in the agroforestry alleys using an anemometer. This additional data would provide a more comprehensive understanding of the microclimatic effects of agroforestry systems.

Moreover, the data indicated that the forested alleys exhibited a more pronounced reaction to rainfall. The immediate increase in soil moisture at a depth of 8 cm was 7% higher than in the agricultural strips. However, this replenished soil moisture was quickly exhausted within two weeks, dropping below the levels observed in the agricultural strips. This rapid depletion is likely attributable to the high

transpiration rates in the forested alleys, particularly within the understory vegetation, as noted by Caubel et al. (2003) and Sahin et al. (2016).

Despite the more pronouced soil moisture depletion in the tree rows of the agroforestry system at Amálie, they also displayed a more efficient recharge mechanism following substantial rainfall. This is attributed to enhanced infiltration due to preferential flow, a phenomenon also observed in a study by Basche and DeLonge (2017). To provide additional support for this hypothesis, it would be essential to evaluate the influence of agroforestry systems on the soil's physical and biochemical properties. This could be achieved by measuring parameters such as infiltration, soil bulk density, and porosity over the trees' maturation period.

It is important to note that this research is focused on the early phases after the implementation of the agroforestry system. As the system matures, it has the potential to become more resilient to the adverse effects of climate change. It is therefore important to continue to monitor the temperature and soil moisture regimes in the upcoming years.

9. REFERENCES

Allen M. F., 2007: *Mycorrhizal Fungi: Highways for Water and Nutrients in Arid Soils*. Vadose Zone Journal 6: 291–297.

Al-Kaisi M. M., Lal R., Olson R. K., Lowery B., 2017: *Fundamentals and functions of soil environment*. In: Al-Kaisi M. M., Lowery B. (eds.): Soil Health and Intensification of Agroecosystems. Academic Press, Cambridge, 400 pp.

Anderson S. H., Udawatta R. P., Seobi T., Garrett H. E., 2009: *Soil water content and infiltration in agroforestry buffer strips*. Agroforestry Systems 75: 5−16.

Arenas-Corraliza M. G., López-Díaz M. L., Moreno G., 2018: *Winter cereal production in a Mediterranean silvoarable walnut system in the face of climate change*. Agriculture, Ecosystem and Environment 264: 111-118.

Baker T. P., Marais Z. E., Davidson N. J., Worledge D., Mendham D. S., 2021: *The role of open woodland in mitigating microclimatic extremes in agricultural landscapes*. Ecological Management and Restoration 22: 118-126.

Barrios E., Shepherd K., Sinclair F., 2015: *Soil health and agricultural sustainability: The role of soil biota*. Agroecology for Food Security and Nutrition: Proceedings of the FAO International Symposium: 104-122.

Basche A., DeLonge M., 2017: *The impact of continuous living cover on soil hydrologic properties: A meta-analysis*. Soil Science Society of America Journal 81: 1179-1190.

Bayala J, Prieto I., 2020: *Water acquisition, sharing and redistribution by roots: applications to agroforestry systems*. Plant and Soil 453: 17–28.

Beillouin D., Schauberger B., Bastos A., Ciais P., Makowski D., 2020: *Impact of extreme weather conditions on European crop production in 2018*. Philosophical Transactions of the Royal Society B: Biological Sciences 375.

Bockheim J., Hartemink A., 2017: *The Soils of Wisconsin*. University of Wisconsin, Madison, 396 pp.

Bond, B. J., Meinzer, F. C., Brooks, J. R., 2007: *How trees influence the hydrological cycle in forest ecosystems*. In: Wood P., Hannah D. M., Sadler J. (eds.), Hydroecology and Ecohydrology: Past, Present and Future. John Wiley & Sons: 7–35.

Bosi C., Pezzopane J. R. M., Sentelhas C. P., 2020: *Silvopastoral system with Eucalyptus as a strategy for mitigating the effects of climate change on Brazilian pasturelands*. Anais da Academia Brasileira de Ciências 92(1).

Brandle J. R., Hodges L., Zhou X. H., 2004: *Windbreaks in North American agricultural systems*. In: Nair P. K. R., Rao M. R., Buck L. E. (eds), New vistas in agroforestry: A compendium for 1st World Congress of Agroforestry. Springer, Dordrecht: 65–78.

Cadisch G., Willington P., Suprayogo D., Mobbs C. D., van Noordwijk M, Rowe C. W., 2004: *Catching and competing for mobile nutrients in soil*. In: van Noordwijk M., et al. (eds): Below ground interactions in tropical agroeceosystems. CABI Publishing: 171-192.

Caubel V., Grimaldi C., Merot P., Grimaldi M., 2003: *Influence of a hedge surrounding bottomland on seasonal soil-water movement*. Hydrological Processes 17: 1811–1821.

Chotte J. L., 2005: *Importance of microorganisms for soil aggregation*. In: Buscot F., Varma A. (eds): Microorganisms in soils: roles in genesis and function. Springer, Berlin: 105-119.

Ciric V., Manojlovic M., Nesic Lj., Belic M., 2012: *Soil dry aggregate size distribution: effects of soil type and land use*. Journal of Soil Science and Plant Nutrition 12(4): 689-703.

Cleugh A. H., 1998: *Effects of windbreaks on airflow, microclimates and crop yields*. Agroforestry Systems 41: 55-84.

Costa P. M. O., de Araújo M. A. G., de Souza-Motta C. M., Malosso E., 2017: *Dynamics of leaf litter and soil respiration in a complex multistrata agroforestry system, Pernambuco, Brazil*. Environment, Development and Sustainability 19(4): 1189–1203.

Coussement T., Maloteau S., Pardon P., Artru S., Ridley S., Javaux M., Garré S., 2018: *A tree-bordered field as a surrogate for agroforestry in temperate regions: Where does the water go?* Agricultural Water Management 210: 198-207.

Cubera E., Moreno G., 2007: *Effect of single Quercus ilex trees upon spatial and seasonal changes in soil water content in dehesas of central western Spain*. Annals of Forest Science 64: 355–364.

Cunningham R. A., 1988: *Genetic improvement of trees and shrubs in windbreaks*. Agriculture, Ecosystems and Environment 22-23: 483-498.

ČGS, 2024: (online) [cit. 2024.03.25], <https://mapy.geology.cz/geo/>

ČHMU, 2023: Územní teploty (online) [cit. 2024.03.25], available at <https://www.chmi.cz/historicka-data/pocasi/uzemni-teploty>

ČÚZK, © 2010: ZABAGED ® - Výškopis - Vrstevnice (online) [cit. 2024.03.25], available at <https://geoportal.cuzk.cz/(S(ip1jwprclt4jxjv2d1o5ozn1))/Default.aspx?mode=TextMeta&side=vyskopis&metadataID=CZ-CUZK-VRSTEVNICE_DMR5G&mapid=8&head_tab=sekce-02-gp&menu=304>

DaMatta F. M., Rahn E., Läderach P., Ghini R., Ramalho J. C., 2019: *Why could the coffee crop endure climate change and global warming to a greater extent than previously estimated?* Climatic Change 152(1): 167-178.

Das S., Sharangi A. B., 2018: *Impact of climate change on spice crops*. Indian spices: The legacy, production and processing of India's treasured export: 397-404.

Doran J. W., Smith M. S., 1987: *Organic matter management and utilization of soil and fertilizer nutrients*. In: SSSA (ed.): Soil Fertility and Organic Matter as Critical Components of Production Systems. SSA, Madison: 55-72.

Everson C. S., Everson T. M., van Niekerk W., 2009: *Soil water competition in a temperate hedgerow agroforestry system in South Africa*. Agroforestry Systems 75: 211–221.

Foth H., 1990: *Fundamentals of soil science 8e*. John Wiley & Sons, Hoboken, 360 pp.

Frelih-Larsen A., Riedel A., Scheidt A., Oluwatoyin A., Gattinger A., Niether W., 2022: *Silvoarable Agforoforestry*. Umwelt Bundesamt, Dessau-Roßlau, 9 pp.

Galloso-Hernández M. A., Rodríguez-Estévez V., Alvarez-Díaz C. A., Soca-Pérez M., Dublin D., Iglesias-Gómez J., Simon Guelmes I., 2020: *Effect of silvopastoral systems in the thermoregulatory and feeding behaviors of water buffaloes under different conditions of heat stress*. Frontiers in Veterinary Science 7.

Gateau-Ray L., Tanner E. V. J. Rapidel B., Marelli J. P., Royaert S., 2018: *Climate change could threaten cocoa production: Effects of 2015-16 El Niño-related drought on cocoa agroforests in Bahia, Brazil*. PLoS One 13(7).

Gerrard J., 2000: *Fundamentals of soils*. Routledge, London, 230 pp.

Gosme M., Dufour L., Inurreta-Aguirre H., Dupraz C., 2016: *Microclimatic effect of agroforestry on diurnal temperature cycle.* In: Presented at the Third European Agroforestry Conference, Montpellier: 183-186.

Grebner L. D., Bettinger P., Siry P. J., Boston K., 2021: *Common Forestry Practices*. In: Introduction to Forestry and Natural Resources (2). Academic Press, Cambridge: 265-294.

Guo H., Zhao Y., 2021: *Using isotopic labeling to investigate root water uptake in an alley cropping system within Taklimakan Desert Oasis, China*. Agroforest Systems 95(1).

Heitman J. L., White J. G., 2014: *Soil Management Can Maximize Water Availability* (online) [cit. 2024.02.18], accessed from <https://content.ces.ncsu.edu/soil-management-can-maximize-water-availability>.

Hesslerová P., Pokorný J., Brom J., Rejšková -Procházková A., 2013: *Daily dynamics of radiation surface temperature of different land cover types in a temperate cultural landscape: Consequences for the local climate*. Ecological Engineering 54: 145-154.

Hillel, D. 2004: *An Introduction to Environmental Soil Physics*. Elsevier Science, San Diego, 494 pp.

Horrigan L., Lawrence R. S., Walker P., 2002: *How sustainable agriculture can address the environmental and human health harms of industrial agriculture*. Environmental Health Perspectives 110: 445-456.

Howe J., Smith P., 2021: *The Soil Habitat*. In: Gentry T., Fuhrmann J., Zuberer D. (eds): *Principles and Applications of Soil Microbiology 3*. Elsevier, Amsterdam. 23-55 pp.

Inurreta-Aguirre H. D., Lauri P. É., Dupraz C., Gosme M., 2018: *Yield components and phenology of durum wheat in a Mediterranean alley-cropping system*. Agroforestry Systems 92(4): 961-974.

Islam N., Wallender W. W., Mitchell J., Wicks S., Howitt R. E., 2006: *A comprehensive experimental study with mathematic modeling to investigate the effects of cropping practices on water balance variables*. Agricultural Water Management 82(1-2): 129-147.

Jacobs R. S., Webber H., Neither W., Grahmann K., Lüttschwager D., Schwartz C., Breuer L., Bellingrath-Kimura D. S., 2022: *Modification of the microclimate and water balance through the integration of trees into temperate cropping systems*. Agricultural Meteorology 323.

Janeček M. et al., 2008: *Základy erodologie*. Skriptum. Česká Zemědělská Univerzita, Prague, 173 pp.

Johnson M. S., Lehmann J., 2006: *Double-funneling of trees: Stemflow and root-induced preferential flow*. Ecoscience 13: 324–333.

Jose S., 2009: *Agroforestry for ecosystem services and environmental benefits: an overview*. Agroforestry Systems 76: 1-10.

Jose S., Gillespie A. R., Seifert J. R., Biehle D. J., 2000: *Defining competition vectors in a temperate alley cropping system in the midwestern USA: 2. Competition for water.* Agroforestry Systems 48: 41-59.

Kanzler M., Böhm C., Mirck J., Schmitt D., Veste M., 2019: *Microclimate effects on evaporation and winter wheat (Triticum aestivum L.) yield within a temperate agroforestry system*. Agroforestry Systems 93: 1821–1841.

Karki U., Goodman M. S., 2015: *Microclimatic differences between mature loblolly-pine silvopasture and open-pasture*. Agroforestry Systems 89: 319-325.

Kay S., Crous-Duran J., Ferreiro-Domínguez N., García de Jalón, S., Graves A., Moreno G., Mosquera-Losada M. R., Palma, J. H. N., Roces-Díaz J. V., Santiago-Freijanes J. J., Szerencsits E., Weibel R., Herzog F., 2018: *Spatial similarities between European agroforestry systems and ecosystem services at the landscape scale*. Agroforestry Systems 92: 1075-1089.

Keysight Technologies, 2023: *FlexDCA User's Guide* (online) [cit. 2024.02.25], accessed from <https://rfmw.em.keysight.com/digitalphotonics/flexdca/ug/content/topics/tdr-tdt-mode/Reference/b_tdr_concepts.htm>

Klamerus-Iwan A., 2014: *Different views on tree interception process and its determinants*. Forest Research Papers 75: 291–300.

Kutílek M., 1978: *Vodohospodářská pedologie*. Státní nakladatelství technické literatury, Prague, 295 pp.

Kutílek M., Kuráž V., Císlerová M., 2004: *Hydropedologie 10*. České vysoké učené technické v Praze, Prague, 176 pp.

Kutílek M., Nielsen D. R., 1994: *Soil Hydrology*. Catena, Cremlingen-Destet, 370 pp.

Lawson G., Dupraz C., Watt'e J., 2019: *Can silvoarable systems maintain yield, resilience, and diversity in the face of changing environments?* In: Lemaire G., Carvalho P. C. D. F., Kronberg S., Recous S. (eds): Agroecosystem Diversity. Academic Press: 145-168.

Lehnert M., 2014: *Factors affecting soil temperature as limits of special interpretation and simulation of soil temperature*. Acta Universitatis Palackianae Olomucensis – Geographica 45(1): 5-22 pp.

Lhotský J., 2000: *Zhutňování půd a opatření proti němu*. Ústav zemědělských a potravinářských informací, Prague, 61 pp.

Ling Q., Gao X., Zhao X., Huang J., Li H., Li L., Sun W., Wu P., 2017: *Soil water effects of agroforestry in rainfed jujube (Ziziphus jujube Mill.) orchards on loess hillslopes in Northwest China*. Agriculture, Ecosystems and Environment 247: 343-351.

Li Y. C., Alva A. K., Calvert D. V., Zhang M., 1997: *Stem flow, throughfall, and canopy interception of rainfall by citrus tree canopies*. HortScience 32: 1059–1160.

Lojka B., Martiník A., Weger J., Houška J., Doležalová H., Kala L., Szábo P., Kotrba R., Krčmářová J., Chládová J., Vávrová K., Jobbiková J., Ehrenbergová L., Snášelová M., Králík T., 2020: *Zavádění agrolesnických systémů na zemědělské půdě*. Česká zemědělská univerzita v Praze, Prague, 72 pp.

Lüttger A. B., Feike T., 2018: *Development of heat and drought related extreme weather events and their effect on winter wheat yields in Germany*. Theoretical and Applied Climatology 132: 15-29.

Martin-Chave A., Béral C., Mazzia C., Capowiez Y., 2019: *Agroforestry impacts the seasonal and diurnal activity of dominant predatory arthropods in organic vegetable crops*. Agroforestry Systems 93: 2067–2083.

Mbow C., Smith P., Skole D., Duguma L., Bustamante M., 2014: *Achieving mitigation and adaptation to climate change through sustainable agroforestry practices in Africa*. Current Opinion in Environmental Sustainability 6: 8-14.

McVicar T. R., et al., 2012: *Global review and synthesis of trends in observed terrestrial near-surface wind speeds: Implications for evaporation*. Journal of Hydrology 416- 417: 182–205.

Moreno G., Obrador J. J., Garcia E., Cubera E., Montero M., Pulido F., Dupraz C., 2007: *Driving competitive and facilitative interactions in oak dehesas through management practices*. Agroforestry Systems 70: 25-40.

Muchane N. M., Sileshi W. G., Gripenberg S., Jonsson M., Pumariño L., Barrios E., 2020: *Agroforestry boosts soil health in the humid and sub-humid tropics: A meta – analysis*. Agriculture, Ecosystems and Environment 295.

Mulia R., Dupraz C., 2006: *Unusual fine root distributions of two deciduous tree species in southern France: What consequences for modelling of tree root dynamics.* Plant Soil 281: 71-85.

Nair R. P., 1993: *An Introduction to Agroforestry*. Kluwer Academic Publishers, Dordecht, 496 pp.

Nair R. P., 2007: *The coming of age of agroforestry*. Journal of the Science of Food and Agriculture 87: 1613-1619.

Nair R. P., Garrity D., 2012: *Agroforestry – The Future of Global Land Use*. Springer, Dordrecht, 542 pp.

Němeček J., Smolíková L., Kutílek M., 1990: *Pedologie a paleo-pedologie*. Československá akademie věd, Prague, 545 pp.

Nerlich K., Graeff-Hönninger S., Claupein W., 2013: *Agroforestry in Europe: a review of the disappearance of traditional systems and development of modern agroforestry practices, with emphasis on experiences in Germany*. Agroforestry Systems 87: 475-492.

Němeček J., Vavříček D., Macků J., Vokoun J., Smejkal J., Prachal J., Kusbach A., Nikl J., 2002: *Taxonomický klasifikační system půd v ČR v lesnické praxi*. Ústav pro hospodářskou úpravu lesů, Brandýs nad Labem, 44 pp.

Nuberg K. I., 1998: *Effects of shelter on temperate crops: a review to define research for Australian conditions*. Agroforestry Systems 41: 3-34.

Nuberg K. I., George B., Reid R., 2009: *Agroforestry for Natural Resource Management*. CSIRO Publishing, 360 pp.

NRCS-USDA, 2006: *Keys to soil taxonomy*. United States Department of Agriculture, National Resources Conservation Service, Washington D. C., 332 pp.

Paul C., Weber M., Knoke T., 2017: *Agroforestry versus farm mosaic systems – Comparing land-use efficiency, economic returns and risks under climate change effects*. Science of the Total Environment 587-588: 22-35.

Pavlásek J., Jačka L., 2014: *Hydropedologie*. Česká zemědělská univerzita, Prague, 104 pp.

Pavlů L., 2018: *Základy pedologie a ochrany půdy*. Česká zemědělská univerzita, Prague, 78 pp.

Petzold R., Feger K. H., Schwärzel, K., 2009: *Wasserhaushalt von Kurzumtriebsplantagen*. In: Reeg T., Bemmann A., Konold W., Murach D., Spieker H. (eds.): Anbau und Nutzung von Bäumen auf Landwirtschaftlichen Flächen. John Wiley & Sons, Ltd., Hoboken: 181-191.

Pidwirny M., Jones S., 2008: PhysicalGeography.net, *Glossary of terms* (online) [cit. 2024.02.06], accessed from<http://www.physicalgeography.net/physgeoglos/a.html>.

Pokorná D., Zabranská J., 2008: *Hydrologie a hydropedologie*. Vysoká škola chemicko-technologická v Praze, Prague.

Ponce M. V., Lohani K. A., Huston T. P., 1997: *Surface Albedo And Water Resources: Hydroclimatological Impact of Human Activities*. Journal of Hydrologic Engineering 4(2): 197-203.

Powlson S. D., Whitmore P. A., Goulding W. T. K., 2011: *Soil carbon sequestration to mitigate climate change: a critical re-examination to identify the true and the false*. Soil Organic Matters 62(1): 42-55.

Prasad M.N.V., Pietrzykowski M., 2020: *Climate Change and Soil Interactions*. Elsevier, Amsterdam, 838 pp.

Qi Z., Helmers M. J., Kaleita A. L., 2011: *Soil water dynamics under various agricultural land covers on a subsurface drained field in north-central Iowa, USA*. Agricultural Water Management 98: 665–674.

Regulation (EU) No 1305/2013: *No 1698/2005* (online) [cit. 2024.03.25], accessed from <https://eur-lex.europa.eu/legal-content/EN/TXT/?uri=celex%3A32013R1305>

Rejšek K., Vácha R., 2018: *Nauka o půdě*. Agriprint, Olomouc, 530 pp.

Reynolds P. E., Simpson J. A., Thevathasan N. V., Gordon A. M., 2007*: Effects of tree competition on corn and soybean photosynthesis, growth, and yield in a temperate tree-based agroforestry intercropping system in southern Ontario, Canada*. Ecological Engineering 29: 362-371.

Richter R., Ballasus H., Engelmann A. R., Zeilhofer C., Sanaei A., Wirth C., 2022: *Tree species matter for forest microclimate regulation during the drought year 2018: disentangling environmental drivers and biotic drivers.* Scientific Reports 12.

Rolo V., Rivest D., Maillard É., Moreno G., 2023: *Agroforestry potential for adaptation to climate change: A soil-based perspective*. Soil Use and Management 39(3): 1006-1032.

Sahin H., Anderson S. H., Udawatta R. P., 2016: *Water infiltration and soil water content in claypan soils influenced by agroforestry and grass buffers compared to row crop management*. Agroforestry Systems 90: 839–860.

Saxton K. E., Rawls W. J., Romberger J. S., Papendick R. I., 1986: *Estimating generalized soil-water characteristics from texture*. Soil Science Society of America Journal 50: 1031-1036.

Schachtschabel P., Blume H. P., Hartge K. H., Schwertmann U., Brümmer G., Renger M., 1984: *Lehrbuch der Bodenkunde*. Enke, Stuttgart, 394 pp.

Sedlmeier K., Feldmann H., Schädler G., 2018: *Compound summer temperature and precipitation extremes over central Europe*. Theoretical and Applied Climatology 131: 1493-1501.

Semnani D., 2016: *Geometrical characterization of electrospun nanofibers*. Isafshan University of Technology, Isafshan, 29 pp.

Sharma G., Partap U., Dahai D. R., Sharma D. P., Sharma E., 2016: *Declining large-cardamom production systems in Sikkim Himalayas: Climate change impacts, agroeconomic potential, and revival strategies*. Mountain Research and Development 36(3): 286-298.

Schoenberger M., Bentrup G., de Gooijer H., Soolanayakanahally R., Sauer T., Brandle J., Zhou X., Current D., 2012: *Branching out: Agroforestry as a climate change mitigation and adaptation tool for agriculture*. Journal of Soil and Water Conservation 67: 128-136.

Spiecker H., Sebasteian H., Makkonen-Spiecker K., Thies M., 2009: *Valuable broadleaved forests in Europe*. Brill, Leiden, 256 pp.

Sposito G., 2018: *The Chemistry of Soils, 3rd ed.* Oxford University, New York, 325 pp.

SPÚ, ©2024: Celostátní database BPEJ (online) [cit. 2024.03.25], available at: <https://www.spucr.cz/bpej/celostatni-databaze-bpej>

Steffan-Dewenter I., Kessler M., Barkmann J., Tscharntke T., 2007: *Tradeoffs between income, biodiversity, and ecosystem functioning during tropical rainforest conversion and agroforestry intensification*. Proceedings of the National Academy of Sciences 104: 4973-4978.

Swieter A., Langhof M., Lamerre J., 2021: *Competition, stress and benefits: Trees and crops in the transition zone of a temperate short rotation alley cropping agroforestry system*. Journal of Agronomy and Crop Science 208(2): 209-224.

Syvitski J. P. M., 1991: *Principles, methods, and application of particle size analysis*. Cambridge University Press, New York, 388 pp.

Šantrůčková H., Kaštovská E., Bárta J., Miko L., Tajovský K., 2018: *Ekologie půdy*. Nakladatelství Jihočeské univerzity, České Budějovice, 260 pp.

Šarapatka B., 2014: *Pedologie a ochrana půdy*. Univerzita Palackého v Olomouci, Olomouc, 232 pp.

Šimek M., 2003: *Základy nauky o půdě: 1. Neživé složky půdy*. Jihočeská Univerzita v Českých Budějovicích, České Budějovice, 131 pp.

Šinko J., Weger J., 2023: *Monitoring mikroklimatických podmínek a hydrického režimu silvoorebného agrolesnického systému – první výsledky*. In: Hnilicová S., Tesař M. (eds): Hydrologie Malého Povodí. Ústav pro hydrodynamiku AVČR, Prague: 131-141.

Taubner H., Roth B., Tippkötter R., 2009: *Determination of soil texture: Comparison of the sedimentation method and the laser-diffraction analysis*. Journal of Plant Nutrition and Soil Science 172(2): 161-171.

Tomášek M., 2007: *Půdy České republiky*. Česká geologická služba, Prague, 67 pp.

Udawatta P. R., Anderson H. S., Gantzer C., Garrett E. H., 2006: *Agroforestry and grass buffer influence on macropore characteristics: A computed tomography analysis*. Soil Science Society of America Journal 70: 1763-1773.

Upson M. A., Burgess P. J., 2013: *Soil organic carbon and root distribution in a temperate arable agroforestry system*. Plant Soil 373: 43-58.

van Noordwijk M., Lawson G., Hairiah K., Wilson J., 2015: Root distribution of trees and crops: competition and/or complementarity. In: Ong C. K., Black C. R.,Wilson, J. (eds.): Tree-Crop Interactions: Agroforestry in a Changing Climate, 2ed. CAB International, Wallingford: 221–257.

van Noordwijk M., Rahayu S., Williams E., Hairiah K., Khasanah N., Schroth G., 2004: *Crop and tree root system dynamics*. In: van Noordwijk M, Cadisch G, Ong CK (eds): Belowground interactions in tropical agroecosystems. CAB International, Waalingford: 83-107.

van Stan J. T., Lewis E. S., Hildebrandt A., Rebmann, C., Friesen, J., 2016: *Impact of interacting bark structure and rainfall conditions on stemflow variability in a temperate beech-oak forest, central Germany*. Hydrological Sciences Journal 61: 2071–2083.

van Wijk W. R., de Vries D. A., 1963: *Periodic Temperature Variations in Homogenous Soil*. In: van Wijk, W.R., (ed): Physics of Plant Environment. Amsterdam.

Vigiak O, Sterk G., Warren A., Hagen J. L., 2003: *Spatial modeling of wind speed around windbreaks*. Catena 52: 273-288.

Vopravil J., 2010: *Půda a její hodnocení v ČR* 1e. Výzkumný ústav meliorací a ochrany půdy, Prague, 148 pp.

Wang Z. H., Fang H., & Chen M., 2017: *Effects of root exudates of woody species on the soil anti-erodibility in the rhizosphere in a karst region, China*. PeerJ 5.

Webber H., Lischeid G., Sommer M., Finger R., Nendel C., Gaiser T., Ewert F., 2020: *No perfect storm for crop yield failure in Germany.* Environmental Research Letters 15.

Weil R. R., Brady N. C., 2016: *The nature and properties of soils*. Pearson Education Limited, Harlow, 1140 pp.

Wild J., Kopecký M., Macek M., Šanda M., Jankovec M., Hasse T., 2019: *Climate at ecologically relevant scales: A new temperature and soil moisture logger for long-term microclimate measurement*. Agricultural and Forest Meteorology 268: 40-47.

Young A., 1997: *Agroforestry for Soil Management*. CAB International, Wallingford, 320 pp.

Zeitoun R., Vandergeest M., Vasava B. H., Machado F. V. P., Jordan S., Parkin G., Wagner-Riddle C., Biswas A., 2021: *In-situ estimation of water retention curve in silt loam and loamy sand soils at different soil depths*. MDPI Physical Sensors 21(2).

10. FIGURE INDEX

11. TABLE INDEX